



Constraints on mantle evolution from Ce-Nd-Hf isotope systematics

Michael Willig^a, Andreas Stracke^{a,*}, Christoph Beier^{b,c}, Vincent J.M. Salters^d

^a *Institut für Mineralogie, Westfälische Wilhelms-Universität Münster, Corrensstrasse 24, 48149 Münster, Germany*

^b *GeoZentrum Nordbayern, Universität Erlangen-Nürnberg, Schloßgarten 5, 91054 Erlangen, Germany*

^c *Department of Geosciences and Geography, University of Helsinki, PO Box 64, FIN-00014, Finland*

^d *National High Magnetic Field Laboratory and Department of Earth, Ocean and Atmospheric Sciences, Florida State University, Tallahassee, FL, USA*

Received 30 September 2019; accepted in revised form 24 December 2019; available online 3 January 2020

Abstract

Mantle evolution is governed by continuous depletion by partial melting and replenishment by recycling oceanic and continental crust. Several important unknowns remain, however, such as the extent of compositional variability of the residual depleted mantle, the timescale, mass flux and composition of recycled oceanic and continental crust. Here, we investigate the Ce-Nd-Hf isotope systematics in a globally representative spectrum of mid ocean ridge and ocean island basalts. Using a Monte Carlo approach for reproducing the observed Ce-Nd-Hf isotope variation shows that the type and age of depleted mantle and recycled crust have the dominant influence on the slope, scatter, and extent of the modeled Ce-Nd-Hf isotope array. The model results suggest a relatively young (<1.5 Ga) average depletion age of the depleted mantle, consistent with Nd and Os isotope model ages of abyssal peridotites, and an apparent moderate extent of incompatible element depletion. The latter, however, is deceiving, because it reflects a natural sampling bias, resulting from melting an inherently heterogeneous depleted mantle. In principal, recycling of oceanic crust can explain most of the isotopic range of the isotopically enriched end of the Ce-Nd-Hf mantle array, but only if the entire compositional variability of the recycled crust is preserved during recycling, residence in the mantle, and re-melting. The latter is unlikely, however, because many sources of internal chemical variance average out on the scale of the bulk oceanic crust, during residence in the mantle, and subsequent sampling by partial melting. Moreover, both the slope and limited scatter of the observed Ce-Nd-Hf mantle array show that recycling of bulk oceanic crust, that is, both the extrusive basalts and intrusive gabbros of the lower oceanic crust must be considered, and are key to better understand crust-mantle cycling in general. The Monte-Carlo simulation also indicates that the return flux from the continental crust into the mantle mainly derives from the lower continental crust, consistent with current models of continental crust evolution, which all require that a substantial amount of the mafic lower continental crust must be recycled into the mantle to maintain the average andesitic composition of the continental crust.

© 2020 Elsevier Ltd. All rights reserved.

Keywords: OIB; MORB; Cerium isotopes; REE; Mantle heterogeneity; Depleted mantle

1. INTRODUCTION

The evolution of Earth's mantle is governed by continuous depletion in incompatible elements through partial melting, and re-enrichment in incompatible elements by recycling oceanic and continental crust (e.g., Hofmann, 1997; Stracke,

* Corresponding author.

E-mail address: astra_01@uni-muenster.de (A. Stracke).

2012, 2018; White, 2015a; Zindler and Hart, 1986). “The part of Earth’s mantle from which basaltic melt has been extracted” and thus has become depleted in incompatible elements is defined as the “depleted mantle” (DM; Allègre, 1982; DePaolo, 1980; Hofmann, 1988; Jacobsen and Wasserburg, 1979; O’Nions et al., 1979; Stracke, 2016). Depleted mantle is probably the main constituent of mid ocean ridge basalt (MORB) mantle sources, but also of most ocean island basalt (OIB) sources, because most OIB sources are characterized by a relative depletion in the highly incompatible elements (Willbold and Stracke, 2006), and they are, on average, isotopically depleted ($\epsilon\text{Nd} \sim +5$, (Kumari et al., 2016)). Therefore, DM constitutes a significant fraction of Earth’s mantle, but its average extent of depletion and mass fraction of the total mantle remain poorly constrained (e.g., Stracke, 2016; Stracke et al., 2019).

The Sr-Nd-Hf-Pb isotope composition of DM is usually inferred from the isotope ratios of MORB. However, the Hf-Nd isotope (e.g., Cipriani et al., 2004; Salters and Dick, 2002; Stracke et al., 2011) and Os isotope ratios of abyssal peridotites (e.g., Alard et al., 2005; Brandon et al., 2000; Day et al., 2017; Harvey et al., 2006; Lassiter et al., 2014; Liu et al., 2008; Snow and Reisberg, 1995; Standish et al., 2002; Warren et al., 2009), as well isotopically ultra-depleted Nd isotope signatures in melt inclusions (Stracke et al., 2019) have revealed the existence of DM that is isotopically more depleted than MORB. Melting of such “ultra-depleted” mantle also explains the increased Hf-Nd isotope variability of MORB compared to OIB (Salters et al., 2011; Sanfilippo et al., 2019), suggesting that ultra-depleted mantle components could be a ubiquitous part of Earth’s mantle. The latter would have far-reaching implications for interpreting the isotopic variation in mantle-derived melts, because it would imply that the rate of mantle depletion and thereby also the rate of mantle-crust exchange could be higher than previously thought (Stracke, 2018; Stracke et al., 2019; 2011). A higher rate of mantle-crust cycling would also decrease the lifetime of different mantle materials, such as depleted mantle and recycled oceanic and continental crust, and thus affect their isotopic evolution.

Here, we use the La-Ce isotope systematics in MORB and OIB to obtain new constraints on the composition and age of DM, but also on the different recycled crustal materials in Earth’s mantle. ^{138}La undergoes branched decay to ^{138}Ba (66%) by electron capture and to ^{138}Ce (34%) by β^- decay. The total half-life of ^{138}La is $\sim 1.03 \times 10^{11}$ years (Sato and Hirose, 1981), and is similar to the half-life of the ^{147}Sm - ^{144}Nd decay system (1.06×10^{11} years; (Begemann et al., 2001)). Cerium isotope ratios in oceanic basalts reflect the time-integrated La/Ce of their mantle source. Because the Nd and Hf isotope ratios reflect the time-integrated Sm/Nd and Lu/Hf of the sampled mantle source, combined Ce-Nd-Hf isotope data reflect the time-integrated rare earth element (REE) patterns of their mantle source. Note that Sm/Hf ratios in oceanic basalts are relatively invariable (Blichert-Toft et al., 1999; Salters and Stracke, 2004), so that La-Ce-Nd-Sm/Hf-Lu accurately define the curvature of the entire REE pattern.

The elements of the three radioactive decay systems La-Ce, Sm-Nd, and Lu-Hf, become increasingly less incompatible in the following order: La, Ce, Nd, Sm \sim Hf, and Lu. Thus, a negative correlation results between La/Ce and Sm/Nd or Lu/Hf for variable products of magmatic differentiation. With time, this behavior also leads to negative correlations in Ce-Nd and Ce-Hf isotope space (Fig. 1, Section 2). Moreover, because Ce is more incompatible than Nd and Hf, Ce/Nd and Ce/Hf vary significantly in different mantle materials, and thus mixing arrays between melts from highly depleted mantle (DM) and any more light rare earth element (LREE) enriched components (e.g., recycled oceanic and continental crust, Willig and Stracke, 2019) are strongly curved in Ce-Nd and Ce-Hf isotope diagrams. The variable extent of LREE depletion, age, and proportion of depleted mantle sources thus considerably influences the slope of the MORB and OIB isotope arrays in Ce-Nd-Hf isotope space, on both local (i.e., at an ocean island or individual ridge segment) and global scales. In contrast, for other combinations of isotope ratios, for example Sr-Nd, mixing arrays are more linear, and their slope is primarily influenced by the isotope composition of the enriched source components.

Cerium isotope ratios, in combination with Nd and Hf isotope ratios, are therefore a unique tracer for identifying variable DM components in the sources of MORB and OIB. But the LREE patterns of different recycled oceanic and continental crust components also lead to distinct Ce-Nd-Hf isotope compositions, especially for recycled lower versus upper continental crust. The Ce-Nd-Hf isotope arrays of oceanic basalts are thus also highly sensitive to the nature and relative proportion of the different recycled crustal materials in their mantle source, on a local and global scale (e.g., Bellot et al., 2015; Willig and Stracke, 2019).

Here, we use a Monte Carlo approach to reproduce the Ce-Nd-Hf mantle array defined by a globally representative, and internally consistent suite of MORB and OIB (Willig and Stracke, 2019). We investigate how mixing melts from different mantle components (DM, recycled oceanic and continental crust) influences the extent and slope of the resulting array in Ce-Nd-Hf isotope space. The different components are allowed to vary in composition and age, resulting in a spectrum of mantle compositions that is sampled by partial melting. Each melting event samples a specific combination of mantle components, and repeated sampling of the compositional spectrum produces a unique modeled Ce-Nd-Hf array. By quantifying how well the modeled arrays fit the observed Ce-Nd-Hf data, we constrain the parameter space that best reproduces the observations with respect to age, composition, and relative proportion of the various mantle materials, and identify the parameters that have the greatest leverage on the extent and slope of the Ce-Nd-Hf array.

2. DEFINING THE Ce-Nd-Hf “MANTLE ARRAYS

High-precision isotope data for MORB and OIB have previously been reported for samples from the Mid-Atlantic and Pacific Ridges and for Iceland, Hawaii, Gough, Tristan da Cunha, St. Helena, Mangaia Island,

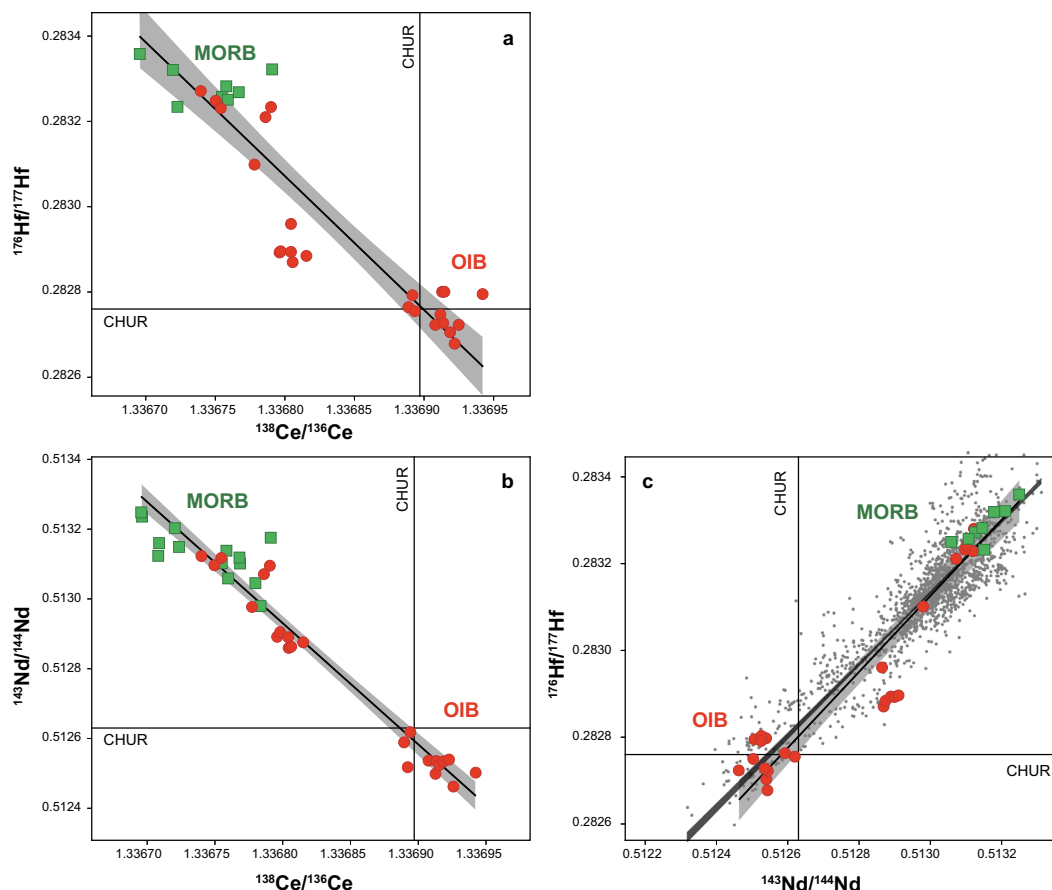


Fig. 1. (a) $^{176}\text{Hf}/^{177}\text{Hf}$ versus $^{138}\text{Ce}/^{136}\text{Ce}$, (b) $^{143}\text{Nd}/^{144}\text{Nd}$ versus $^{138}\text{Ce}/^{136}\text{Ce}$, and (c) $^{176}\text{Hf}/^{177}\text{Hf}$ versus $^{143}\text{Nd}/^{144}\text{Nd}$ diagram for OIB (red dots) and MORB (green squares). Panel (a) and (b) show only data for which combined Ce, Nd and Hf isotopic data exists (supplementary Table 1), panel (c) includes literature data from the compilation provided in [Stracke \(2012\)](#), gray dots). The vertical and horizontal line denote the isotope composition of the chondritic uniform reservoir (CHUR) ([Workman and Hart, 2005](#); [Bouvier et al., 2008](#); [Willig and Stracke 2019](#)). An ordinary least square (OLS) bisector fit (c.f. [Isobe et al., 1990](#)) is shown as a black line with a 2 S.E. envelope in gray. In panel (c) the OLS bisector fit for the literature data ([Stracke, 2012](#), grey dots) is shown in dark grey. (For interpretation of the references to colour in this figure legend, the reader is referred to the web version of this article.)

and McDonald seamount ([Willig and Stracke, 2019](#)). In addition, new Ce-Nd-Hf data for eight additional OIB samples from Gough, St. Helena, and Tristan da Cunha are reported in supplementary Table 1.

The samples for which Ce isotope data exist (supplementary Table 1) cover most of the global Sr-Nd-Pb-Hf isotopic spectrum of MORB and OIB. Their Ce isotope ratios range from about $\epsilon\text{Ce} = -1.5$ ($\epsilon\text{Nd} = 12$, $\epsilon\text{Hf} = 20$) at the depleted end of the spectrum, which is defined by MORB and Icelandic basalts, to $\epsilon\text{Ce} = 0.2$ ($\epsilon\text{Nd} = -3$, $\epsilon\text{Hf} = -3$) on the enriched side, represented by OIB from Gough island, and Tristan da Cunha ([Fig. 1](#), supplementary Table 1). Samples from Mangaia, St. Helena and McDonald seamount are clustered around $\epsilon\text{Ce} = 0.7$ ($\epsilon\text{Nd} = 5$, $\epsilon\text{Hf} = 5$). These HIMU-type OIB have slightly lower ϵHf for a given ϵNd and ϵCe relative to the rest of the samples ([Fig. 1](#)). However, despite this small offset of the HIMU basalts, all Ce-Nd-Hf data define a narrow linear array in Ce-Nd-Hf isotope space, particularly relative to their distribution in Nd-Pb and Nd-Sr isotopic space ([Stracke et al., 2005](#)).

For the combined Ce-Nd-Hf data determined by [Willig and Stracke \(2019\)](#), and this study), which are listed in supplementary Table 1, ordinary least square bisector fits ([Isobe et al., 1990](#)) for the ϵCe - ϵNd - ϵHf data define the slope and intercept of the ϵNd - ϵCe , ϵHf - ϵCe , and ϵHf - ϵNd arrays. The ordinary least square bisector defines the line that mathematically bisects the regression lines of variable Y against X , and X against Y . When both X and Y variables have analytical or inherent uncertainty, the ordinary least square bisector fit is likely the most reliable fitting method for determining the underlying relationship between two variables ([Isobe et al., 1990](#)). This approach results in the following relationships:

$$\begin{aligned} \epsilon^{143}\text{Nd} &= \epsilon^{138}\text{Ce} \times -9.06 \pm 0.35 \text{ (2 S.E.)} - 0.71 \pm 0.60 \text{ (2 S.E.)} \\ \epsilon^{176}\text{Hf} &= \epsilon^{138}\text{Ce} \times -14.84 \pm 0.72 \text{ (2 S.E.)} - 0.62 \pm 1.81 \text{ (2 S.E.)} \\ \epsilon^{176}\text{Hf} &= \epsilon^{143}\text{Nd} \times 1.59 \pm 0.09 \text{ (2 S.E.)} + 0.59 \pm 1.22 \text{ (2 S.E.)} \end{aligned}$$

For calculating the ϵ -values, the CHUR values are from [Bouvier et al. \(2008\)](#) for Nd and Hf ($^{143}\text{Nd}/^{144}\text{Nd} = 0.512630$ and $^{176}\text{Hf}/^{177}\text{Hf} = 0.282785$), and from [Willig and Stracke \(2019\)](#) for Ce ($^{138}\text{Ce}/^{136}\text{Ce} = 1.336897$).

Including the few existing Ce–Nd isotope data for MORB and OIB ([Bellot et al., 2015](#); [Boyet et al., 2019](#); [Dickin, 1988, 1987](#); [Makishima and Masuda, 1994](#); [Tanaka et al., 1987](#)), does not significantly change the slope of the correlation lines defined above. The abundant Nd–Hf literature data (taken from the compilation in [Stracke, 2012](#)) produce a tighter fit, but within error of our more limited combined Ce–Nd–Hf data, and almost identical to the equation defined by [Vervoort and Patchett \(1996\)](#):

$$\epsilon^{176}\text{Hf} = \epsilon^{143}\text{Nd} \times 1.50 \pm 0.03 \text{ (2 S.E.)} + 1.51 \pm 0.24 \text{ (2 S.E.)}.$$

3. Ce–Nd–Hf MANTLE GEOCHEMISTRY

3.1. Ce–Nd–Hf isotope evolution of different mantle components

Evolution of different mantle materials in Ce–Nd–Hf isotope space is a function of their La/Ce, Sm/Nd and Lu/Hf and the time available for isotopic decay.

Depleted mantle (DM, [Salters and Stracke, 2004](#); [Workman and Hart, 2005](#)) for example, evolves high ϵNd and ϵHf , but low ϵCe . The La/Ce, Sm/Nd and Lu/Hf of the DM estimates of [Salters and Stracke \(2004\)](#), and the three different estimates of [Workman and Hart \(2005\)](#) differ significantly, and thus develop significant isotopic differences with time, resulting in distinct vectors in Ce–Nd–Hf isotopic space ([Fig. 2](#)). The compositional differences between these DM estimates result from the different strategies for estimating the incompatible element content of the DM. [Salters and Stracke \(2004\)](#) base their estimate on the composition of LREE-depleted MORB, whereas [Workman and Hart \(2005\)](#) use abyssal peridotites to estimate the REE composition of the DM. Because most abyssal peridotites are variably affected by partial melting and refertilization by melt–rock interaction (e.g., [Brunelli et al., 2014, 2006](#); [Hellebrand and Snow, 2003](#); [Stracke et al., 2011](#); [Warren, 2016](#)), which re-enriches the LREE, the La/Ce (and Ce/Nd, Hf) are comparatively high for given Sm/Nd in the [Workman and Hart \(2005\)](#) estimate. Hence, the [Workman and Hart \(2005\)](#) DM evolves to higher Ce for given Nd and Hf isotope ratios than the [Salters and Stracke \(2004\)](#) DM estimate, resulting in a vector that is steeper than the slope of the observed Ce–Nd and Ce–Hf correlation for the [Workman and Hart \(2005\)](#) estimate, and a vector that is shallower than the slope of the observed Ce–Nd and Ce–Hf correlation for the [Salters and Stracke \(2004\)](#) DM estimate.

Bulk recycled oceanic crust (OC) consists of extrusive MORB and intrusive rocks such as the oceanic gabbros of the lower oceanic crust. Recycled bulk OC, as estimated by [White and Klein \(2014\)](#), generally evolves along the observed ϵNd – ϵCe array to isotopic compositions between DM and recycled upper and lower continental crust

(UCC–LCC; [Fig. 2](#); see more detailed discussion in [Section 5.1](#)), but plots below the observed arrays in ϵHf – ϵCe and ϵHf – ϵNd diagrams ([Fig. 2a, c](#); [Salters and White, 1998](#); [Stracke et al., 2003](#)).

Recycled UCC and LCC ([Rudnick and Gao, 2014](#)) evolve high ϵCe , but low ϵNd and ϵHf . Continental crust components (UCC and LCC) evolve to ϵNd and ϵHf values that are lower than the observed MORB and OIB values, with UCC evolving to even more extreme isotope ratios than LCC for the same age. In the Ce–Hf and Ce–Nd isotope diagrams ([Fig. 2a, b](#)), UCC and LCC evolve towards lower ϵNd and ϵHf for given ϵCe relative to the observed Ce–Nd–Hf array ([Fig. 2](#)). Although the vectors for LCC and recycled bulk OC ([White and Klein, 2014](#)) have similar slopes in Ce–Hf isotopic space, bulk OC generally has more moderate ϵCe and ϵNd values than LCC for any given age. In Ce–Nd isotope space UCC, and especially LCC evolve along vectors with steeper slope than bulk OC, which evolves along a vector parallel to the array formed by MORB and OIB. Especially recycled LCC develops along a vector that is significantly steeper than the observed Ce–Nd(Hf) mantle array, which may allow distinguishing recycled LCC and UCC materials in different mantle sources.

3.2. Generating a Ce–Nd–Hf mantle array by sampling heterogeneous mantle

For interpreting the observed Ce–Nd–Hf mantle array it is important to understand not only how mantle components evolve, but also how partial melting samples these components and how the derivative melts mix to form the erupted melts.

Mixing arrays for melts from DM and more incompatible element enriched source materials (OC, UCC, LCC; [Fig. 3](#)) are generally curved in Ce–Nd and Ce–Hf isotope space. The degree of curvature increases with increasing depletion of the DM (i.e., lower La/Ce and Ce content; [Fig. 3](#)). Although the nature of the enriched source component also has a significant influence, variable curvature mostly results from different DM source components, because the La/Ce and Ce contents in various enriched end-members are much less variable than those of different depleted end-members. Variably depleted mantle can thus be identified by arrays with different position and slopes in Ce–Nd(–Hf) isotope diagrams ([Fig. 3](#)), on both a local and global scale.

On a local scale, the involvement of highly depleted mantle causes strongly curved mixing arrays with melts from an enriched source component. That is, steep slopes on the high ϵCe –low ϵNd – ϵHf side (reflecting low proportions of DM), but shallow, almost horizontal slopes on the low ϵCe –high ϵNd – ϵHf side of the mixing curve (reflecting high proportions of DM, [Fig. 3](#)). Hence, both different DM compositions, but also variable proportions of DM and enriched components can be resolved on a local scale.

On a global scale, the nature of the average DM involved in MORB and OIB genesis controls the steepness of the observed Ce–Nd–Hf mantle array, and could influence whether it intersects the chondritic reference value ([Willig and Stracke, 2019](#)). The slope of the Ce–Nd–Hf man-

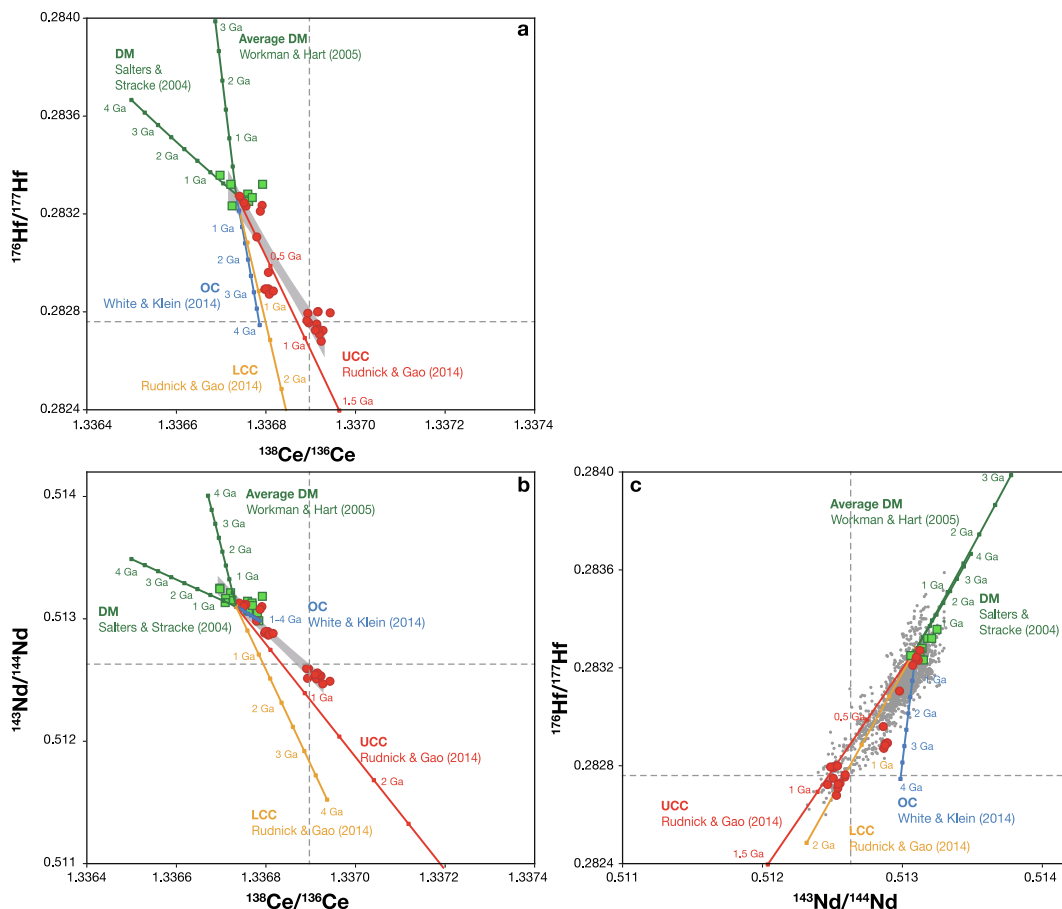


Fig. 2. Isotopic evolution trends for depleted mantle (DM, green), lower continental crust (LCC, orange), upper continental crust (UCC, red) and bulk oceanic crust (OC, blue) in (a) $^{176}\text{Hf}/^{177}\text{Hf}$ versus $^{138}\text{Ce}/^{136}\text{Ce}$, (b) $^{143}\text{Nd}/^{144}\text{Nd}$ versus $^{138}\text{Ce}/^{136}\text{Ce}$, and (c) $^{176}\text{Hf}/^{177}\text{Hf}$ versus $^{143}\text{Nd}/^{144}\text{Nd}$ diagrams, including the OIB and MORB data shown in Fig. 1. The initial isotopic composition of the various end-members is the isotopic composition of the upper mantle at the time of formation, which is approximated by evolving linearly from BSE at 4.56 Ga (i.e., $\varepsilon\text{Ce} = \varepsilon\text{Nd} = \varepsilon\text{Hf} = 0$) to $\varepsilon\text{Ce} = -1.2$, $\varepsilon\text{Nd} = 9.2$, $\varepsilon\text{Hf} = 18.4$ at present (cf. Stracke, 2012 and supplementary Table 1). The decay constants used are given in supplementary Table 2. (For interpretation of the references to colour in this figure legend, the reader is referred to the web version of this article.)

tle array therefore reflects the average composition of DM involved in global MORB and OIB genesis, and thus constrains the average age and extent of depletion of the DM on a global scale.

The shape and extent of the observed Ce-Nd-Hf mantle array is also greatly affected by sampling variably depleted and enriched source components in different proportions. For the mixing curves in Fig. 3, for example, the proportion of melt from the DM source component varies along each mixing line. In contrast, in Fig. 4, the proportion of melts from DM to melts from a recycled component (here consisting of OC and UCC) is kept constant for each individual mixing curve, but the ratio of DM/(OC + UCC) varies between the different mixing curves. Increasing the proportion of melts from the DM elevates the εNd and εHf relative to εCe , and limits the extent of the mixing curve towards the enriched source component (OC + UCC). Hence, for a similar enriched source component, different proportions of melts from a single DM component can lead to parallel mixing trends in Ce-Nd and Ce-Hf space, which

may lead to increasing isotopic variance at the DM end of the arrays, on both local and global scales. Moreover, a relatively large proportion of DM limits the extent of the Ce-Nd-Hf mantle array, and little variance in the proportion of DM limits the variability perpendicular to the array (Fig. 4).

In summary, the geometry of the observed Ce-Nd-Hf mantle array, and that of any local array for a given ocean island or ridge segment, is highly sensitive to the average composition and age of the DM involved. Although the Nd-Hf isotope data in MORB also indicate melting of variably depleted mantle sources (Salters et al., 2011), the Ce isotope data, in combination with Nd and Hf are much more sensitive to variably depleted mantle and thus provide higher resolution for distinguishing different DM components. Combining Ce with Nd and Hf isotope data is therefore a unique tool for identifying the role of variably depleted mantle in MORB and OIB genesis. Moreover, other than for the Nd-Hf data alone, combined Ce-Nd-Hf isotope data allow discriminating between different types

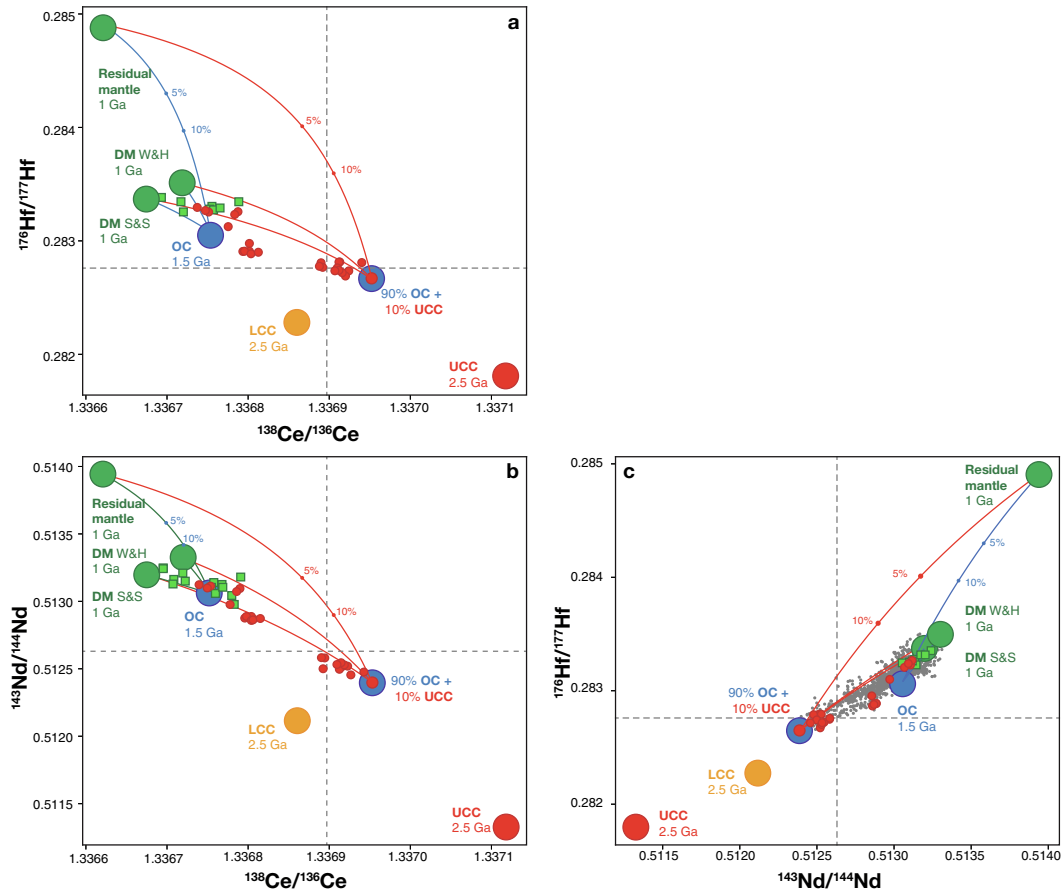


Fig. 3. Diagrams of (a) $^{176}\text{Hf}/^{177}\text{Hf}$ versus $^{138}\text{Ce}/^{136}\text{Ce}$, (b) $^{143}\text{Nd}/^{144}\text{Nd}$ versus $^{138}\text{Ce}/^{136}\text{Ce}$, and (c) $^{176}\text{Hf}/^{177}\text{Hf}$ versus $^{143}\text{Nd}/^{144}\text{Nd}$ show mixing curves between melts from different depleted mantle components in green and a recycled crustal component, which is a 9:1 mixture of recycled bulk oceanic crust (OC; White and Klein, 2014, blue) and recycled upper continental crust (UCC, Rudnick and Gao, 2014, red). The recycling time of oceanic and continental crust is 1.5 Ga. Prior to recycling, the continental crust had a crustal residence time of 1 Ga, hence was formed at 2.5 Ga. The depletion age of the DM is assumed to be 1 Ga, i.e., the recycled components are incorporated during mantle processing into depleted mantle. Tick marks on the mixing curves represent the fraction of crustal melt involved in melt mixing. The depleted components have compositions taken from Salters and Stracke (2004, S&S) or Workman and Hart (2005, W&H). Also shown is a modeled depleted mantle corresponding to a residual mantle column produced by partial melting of DM to 12% (DM, Salters and Stracke, 2004). The latter thus corresponds to highly refractory mantle. (For interpretation of the references to colour in this figure legend, the reader is referred to the web version of this article.)

continental material, and thus add new constraints on the relative importance of recycled LCC and UCC for crust-mantle evolution.

4. MODELING THE Ce-Nd-Hf MANTLE ARRAY

Although the mantle is a complex assembly of many different incompatible element depleted and enriched materials, most of the isotopic variation in oceanic basalts is captured within a simple conceptual framework: depletion by partial melting and replenishment by recycling of the generated oceanic and continental crust back into the mantle (e.g., Hofmann, 1997; Stracke, 2012, 2018; White, 2015a; 2015b; Willbold and Stracke, 2010; Zindler and Hart, 1986). Although the mantle is certainly more complex, mixtures between melts from DM, recycled OC, UCC and LCC can reproduce the general distribution and pattern of the observed Sr-Nd-Hf-Pb isotope ratios (e.g., Stracke, 2012,

2018; White, 1985; 2015a; Willbold and Stracke, 2010; Zindler and Hart, 1986).

Even when simplifying the problem to sampling of only four generic mantle components (DM, OC, LCC, UCC), however, their abundance, compositional variance, and age are unknown. Hence sampling of only four variable components defines a system with many coupled degrees of freedom. Such systems can suitably be investigated with Monte Carlo methods, resulting in reasonable bounds on the range of input parameters, and therefore valuable constraints on the isotopic evolution of Earth's mantle.

4.1. Model framework

4.1.1. Principal model set-up

The observed Ce-Nd-Hf mantle array is modeled by mixing melts from four generic mantle components: DM, recycled bulk OC, recycled UCC and LCC, see description

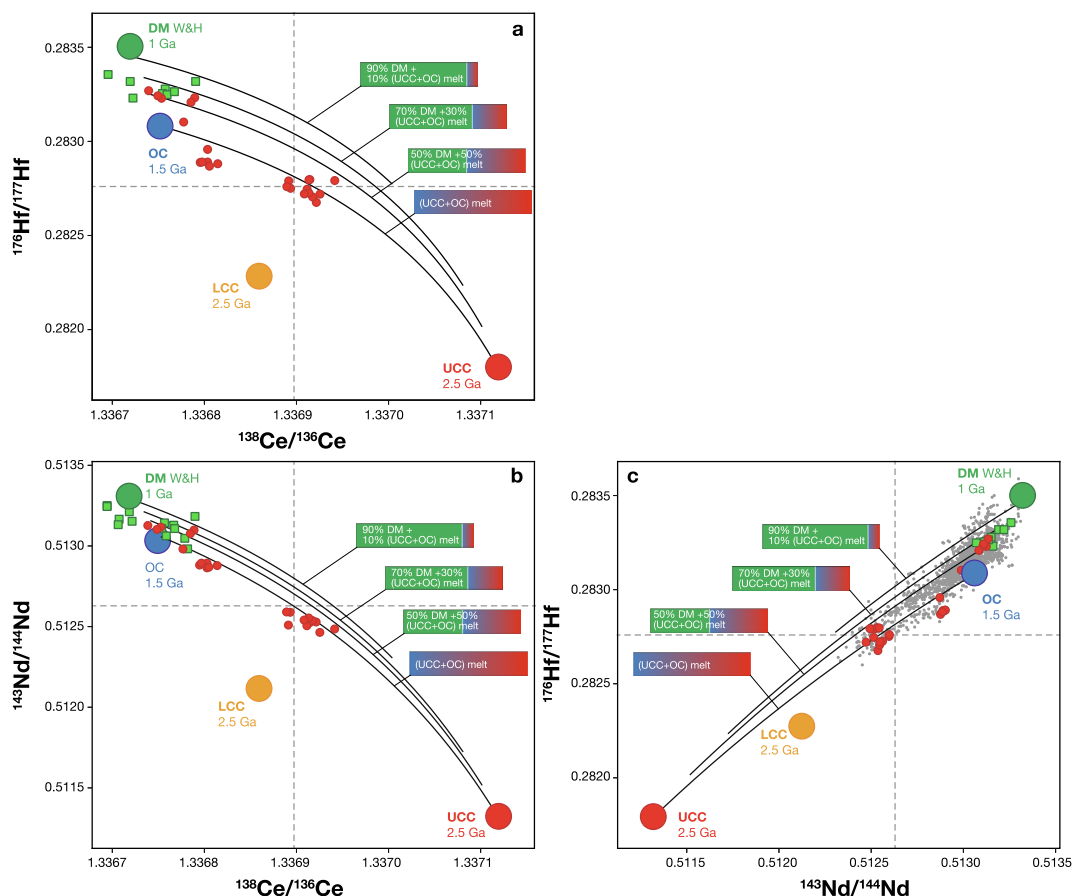


Fig. 4. Diagrams of (a) $^{176}\text{Hf}/^{177}\text{Hf}$ versus $^{138}\text{Ce}/^{136}\text{Ce}$, (b) $^{143}\text{Nd}/^{144}\text{Nd}$ versus $^{138}\text{Ce}/^{136}\text{Ce}$, and (c) $^{176}\text{Hf}/^{177}\text{Hf}$ versus $^{143}\text{Nd}/^{144}\text{Nd}$ show mixing curves between melts from recycled oceanic crust (blue) and upper continental crust (red) and DM (green). The proportion of melts from the DM to melts from a recycled component (here consisting of OC and UCC) is kept constant for each individual mixing curve, but varies between the different mixing curves. The variability along each individual mixing trend is caused by varying the proportion of OC and UCC within the enriched source component. Increasing the proportion of melts from the DM elevates the ε_{Nd} and ε_{Hf} relative to ε_{Ce} , and limits the extent of the mixing curve towards the enriched source component. Different proportions of melts from a single DM component thus result in parallel trends in Ce-Nd and Ce-Hf space, which may lead to increasing isotopic variance at the depleted (DM) end of the isotope arrays on these diagrams. (For interpretation of the references to colour in this figure legend, the reader is referred to the web version of this article.)

of the model set-up and input parameters listed in Table 1. The composition of the DM, OC, UCC, and LCC components is taken from literature estimates (Salters and Stracke, 2004; Workman and Hart, 2005; Rudnick and Gao, 2014; White and Klein, 2014). The different strategies used to account for compositional variability of each component are described in detail in Section 4.1.2. Depending on their age, which is an adjustable input parameter, these components have a given initial Ce-Nd-Hf isotope ratio (Section 4.1.3). The mantle components are then melted, and melts from all four components are mixed together, resulting in a single model point (Section 4.1.4). The Ce-Nd-Hf isotope ratios of this model point depend on the specific composition, age and the relative abundance of the four mantle components (4.1.5). By repeating the process for the same input parameters within the defined compositional variance (Section 4.1.2), and the chosen variance for the age and proportion of the four mantle components (Sections 4.1.3–4.1.5), a discrete number of model points is created,

which taken together, define a (single) modeled Ce-Nd-Hf mantle array. Using 60 iterations proved to be a good number for computational efficiency and for having a large-enough number of model points to define a modeled Ce-Nd-Hf mantle array, which thus typically consists of 60 model points. Finally, a goodness of fit algorithm is used to assess to what extent the modeled Ce-Nd-Hf mantle array reproduces the observed data (Section 4.2, supplementary table 1).

4.1.2. Composition and variability of mantle components

The composition of the DM varies in the model, with equal probability, between the estimates of Salters and Stracke (2004), and the three different estimates of Workman and Hart (2005).

To model recycling of bulk OC, we use the median composition by White and Klein (2014). The assigned compositional variance reflects differences of $\pm 1\%$ (S.D.) in the average degree of partial melting of a uniform bulk OC

Table 1
Principal model set up and input parameters.

	DM	OC	UCCLCC	details
Input composition (La, Ce, Sm, Nd, Lu, Hf) uncertainty	Salters and Stracke (2004) Workmann and Hart (2005) See Section 4.1.2	White and Klein (2014)	Rudnick and Gao (2014)	Section 4.1.2
Age	T_{DM}	$T_{recycling}$	$T_{recycling} + T_{residenceCC}$	Section 4.1.3
Uncertainty	Adjustable input variable			
$R_{initial}$ (Ce, Nd, Hf)	$R_{initial} (T_{DM})$	$R_{initial} (T_{recycling})$	$R_{initial} (T_{recycling} + T_{residenceCC})$	
Degree of melting F [%]	20	100		Section 4.1.4
Source OC /DM	Input variable, but < 3/7			Section 4.1.5
Uncertainty	Adjustable input variable			
Source (UCC + LCC)/OC	Input variable, min–max: 0–1			
Uncertainty	Adjustable input variable			
Source LCC/(UCC + LCC)	Input variable, min–max: 0–1			
Uncertainty	Adjustable input variable			

source (cf. Langmuir et al., 1992). As such the model captures geochemical variability between segments of oceanic crust produced at mid oceanic ridges with variable thermal profiles, or similar degrees of melting of compositionally variable bulk OC sources.

The UCC and LCC are the average estimates given by Rudnick and Gao (2014), and have no compositional variance assigned. Upper continental crust is recycled into the mantle after continental erosion, transportation, sedimentation, and subduction. All these processes average, and thus minimize the enormous compositional spectrum of the recycled UCC, as evidenced by the striking similarity of average subducted sediment (GLOSS, Plank, 2014) and UCC (Rudnick and Gao, 2014). Rather than assigning an arbitrary compositional variance to the UCC, compositional variance in the recycled continental crust is thus captured by varying the proportion of UCC and LCC.

4.1.3. Age of the mantle components

All mantle end-members are allowed to vary in age between 0 and 4.56 Ga. At the time of their formation, all four components (DM, bulk OC, LCC, and UCC) derive from, and thus inherit the isotopic composition of the upper mantle. The isotope evolution of the upper mantle is approximated by evolving linearly from bulk silicate earth at 4.56 Ga to an average MORB isotope ratio at the present time (i.e., $\epsilon_{Ce} = \epsilon_{Nd} = \epsilon_{Hf} = 0$ to $\epsilon_{Ce} = -1.2$, $\epsilon_{Nd} = 9.2$, $\epsilon_{Hf} = 18.4$; (Stracke, 2012) and supplementary Table 1).

The age of the DM component is the age of its last depletion, i.e., the time at which this component has acquired its assumed composition by melt extraction from the upper mantle.

The age of recycled bulk OC is the recycling or mantle residence time, which in this model equals the recycling time of the continental crust (UCC and LCC). However, both continental crust components reside, and hence develop isotopically in the continental crust, before being recycled into the mantle. The age of the crustal materials thus is the sum of their residence time in the crust and man-

tle. Implicit in the model therefore is that the average age of the recycled OC is lower than the formation age of the recycled UCC and LCC. This is an emergent feature of decomposing the UCC-LCC and OC ages into a crustal residence time (only experienced by UCC and LCC) and mantle residence or recycling time (cf. Stracke et al., 2003). A simplifying assumption is that the mean ages for the recycled UCC and LCC are equal. Although this is unlikely to be the case in nature, varying the age of the recycled UCC relative to LCC has a similar effect on the isotope ratios of the total continental crust (UCC and LLC) as varying the proportion of UCC and LCC. It is therefore not explored separately.

4.1.4. Melting and mixing of mantle components

During sampling by oceanic volcanism, the DM and the recycled crustal components (OC, LCC and UCC) melt to a large-enough extent that Ce, Nd and Hf are quantitatively extracted into the melt. About 90% of the Hf is incorporated in the melt after 6% fractional melting of DM and 99% is extracted after melting to 10%. For Ce and Nd, which are more incompatible than Hf, quantitative extraction from source to melt occurs at even lower degrees of melting. In our model the DM melts to maximum of 20%, and thus the relative abundance of Ce-Nd-Hf is very similar to those in the DM components used in the model (Section 4.1.3). Compared to the extent of melting of ca. 10% estimated in previous studies (cf. Langmuir et al., 1992) the high degree of melting for the DM assumed here has a negligible effect on the relative abundances of Ce-Nd-Hf in the melt and hence a small effect on the mixing trends with more enriched source components, that is, they become slightly less curved and thus the scatter of the modeled Ce-Nd-Hf mantle array is reduced. Rather than varying the extents of melting to approximate the compositional variability of melts from the DM, we vary the DM source composition as described in Section 4.1.2 above, which has a similar effect. More incompatible element enriched recycled components (OC, UCC, LCC) melt to an even larger extent than the peridotitic DM (e.g.,

Lambart et al., 2016; Pertermann and Hirschmann, 2003), which also leads to quantitative extraction of Ce, Nd and Hf into the produced melts. A simplifying assumption in the model therefore is that OC, UCC, LCC melt completely. The melts from each component (DM, OC, UCC, LCC) then mix to form a basalt that is plotted as one of the 60 total points of the modeled Ce-Nd-Hf mantle array.

4.1.5. The modeled Ce-Nd-Hf mantle array

Any specific modeled Ce-Nd-Hf mantle array, that is, one model solution, is calculated assuming a mean, standard deviation (S.D.), minimum and maximum value for the following parameters: the age of the DM, the recycling time of crustal components in the mantle, the continental residence time (age of the recycled UCC, LCC = continental residence time + mantle residence time), the sampling ratio of OC/DM, OC/(UCC + LCC), and the proportion of LCC in the recycled total continental crust, LCC/(LCC + UCC) (see Tables 1 and 2).

Each of the parameters have minimum and maximum values assigned. The ages of the mantle components are between 4.56 and 0 Ga. The sampling proportions are ≥ 0 , and the ratio of recycled OC to DM (OC/DM) in the source is limited to (3/7) (Sobolev et al., 2007), with a mean $\leq 1/4$. This restriction is reasonable when compared to estimates of how much oceanic crust has been produced at oceanic ridges over Earth's history (e.g., Salters and Stracke, 2004; Stracke et al., 2003; Tackley, 2015). In the simplest case, assuming that the entire mantle has melted in Earth's history and that oceanic crust production reflects about 10% of partial melting, OC/DM = 1/9, which is significantly less than the maximum OC/DM $\sim 1/4$ used here. The model thus allows for a considerable range of OC/DM, acknowledging that OC/DM in individual mantle sources could be larger or smaller than expected, on average, for the entire mantle.

4.2. Exploration of model parameter space

One exemplary of many possible model solutions is shown in Fig. 5 and the associated input variables are listed in Table 2. To evaluate what constraints the model provides on the input parameters (Tables 1 and 2), and thus on mantle evolution, requires identifying which of the modeled arrays reproduce the observed Ce-Nd-Hf array better than others. The latter is done by quantifying the goodness of fit between the modeled and observed Ce-Nd-Hf mantle array.

The goodness of fit algorithm used here is a measure for the average squared distance in isotopic space from mod-

eled basalts to the closest observed oceanic basalt and vice versa. Using this algorithm, the best possible score is 0, which is obtained when the modeled mantle array is identical to the observed Ce-Nd-Hf mantle array. Similar results are obtained using an alternative scoring algorithm based on the isotopic composition of, and variance in the mantle end-members. The working, suitability, and validation of different scoring algorithms is further elaborated on in the supplementary materials.

Having a metric for the goodness of fit allows exploration of the parameter space systematically. This is done by selecting two controlled variables of interest and assigning unique values to them, for example the age of the DM and the age of the bulk OC. Other variables (Tables 1 and 2) are allowed to vary and are adjusted to optimize the goodness of fit score using a gradient descent algorithm. The goodness of fit scores obtained after optimization represent the best fit obtainable for these two chosen controlled variables. Performing this operation for different combinations of values for the controlled variables allows identifying combinations of input parameters that produce a better fit than others, and illustrating these results in diagrams such as Figs. 6–8.

Parameters of interest that are explored are the age of the DM, the recycling time of crustal materials (OC, LCC, UCC) in the mantle and the sampling ratio of recycled LCC/(LCC + UCC); Table 2). To investigate the former two, all possible combinations (7×7) for the following ages are taken for the DM and recycled crust (OC, LCC, UCC): 0.5 ± 0.25 , 1 ± 0.5 , 1.5 ± 0.75 , 2 ± 1 , 2.5 ± 1.25 , 3 ± 1.5 , 3.5 ± 1.75 Ga (1 S.D.). For each combination the other parameters (sampling proportions, continental crust residence time) are tuned by gradient descent. The optimized scores reflect how consistent each modeled array is with the observed Ce-Nd-Hf data, for a given average DM age and crustal recycling time (Fig. 6).

To investigate the sensitivity of the mantle array to the ratio of recycled LCC/(LCC + UCC) sampled in the mantle, a similar routine is performed where the age of the DM and the sampling ratio of recycled LCC/(LCC + UCC) are controlled and the other parameters are optimized by gradient descent (Fig. 8).

4.3. Model results

4.3.1. Age of the DM, recycled OC, and recycling of LCC vs. UCC

Optimized goodness of fit scores as a function of the age of the DM and age of the recycled crust (OC, UCC, LCC)

Table 2
Input parameters used to generate Fig. 5.

Attribute	Mean	S.D.	min	max
Continental crust residence time [Ga]	0.18	0.3	0	4
Recycling time [Ga]	2	1	0	4
Age DM [Ga]	1	0.5	0	4
Source LCC/(UCC + LCC)	0.72	0.02	0	1
Source CC/OC	0.07	0.1	0	1
Source OC/DM	0.19	0.01	0.01	3/7
Number basalts modeled	150	–	–	–

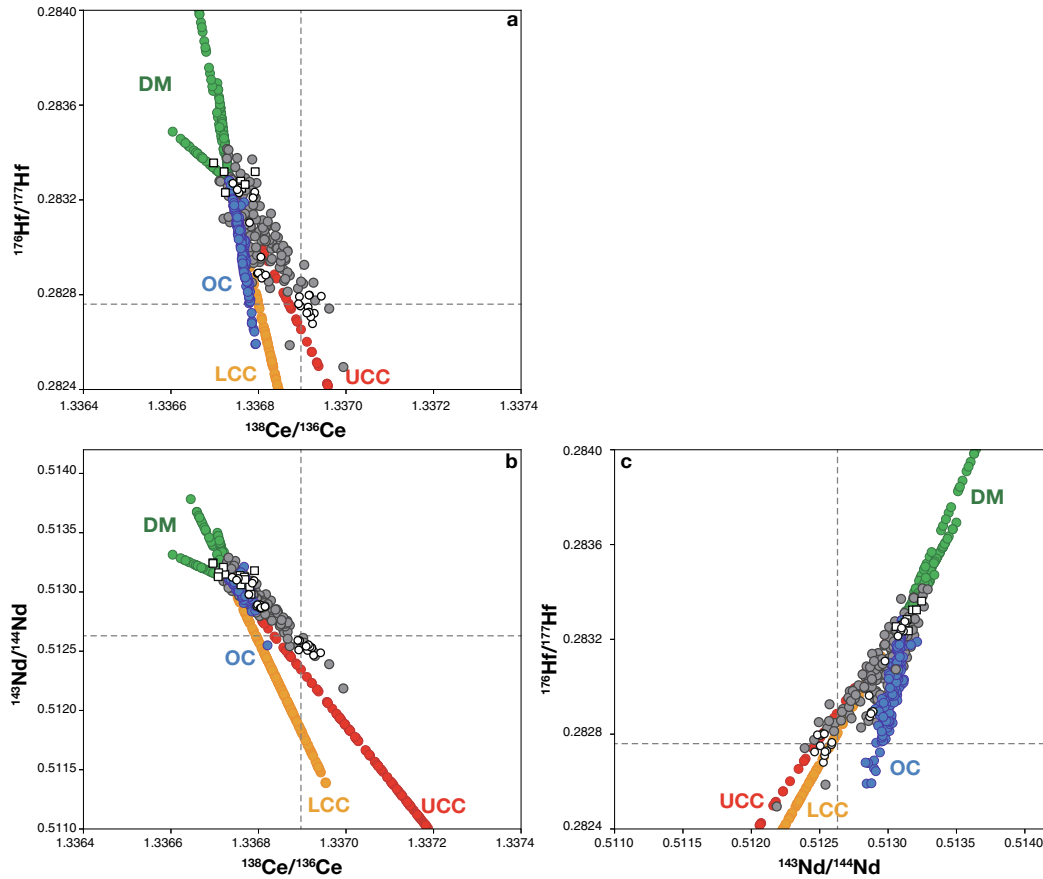


Fig. 5. Diagrams of (a) $^{176}\text{Hf}/^{177}\text{Hf}$ versus $^{138}\text{Ce}/^{136}\text{Ce}$, (b) $^{143}\text{Nd}/^{144}\text{Nd}$ versus $^{138}\text{Ce}/^{136}\text{Ce}$, and (c) $^{176}\text{Hf}/^{177}\text{Hf}$ versus $^{143}\text{Nd}/^{144}\text{Nd}$ show an exemplary model output for the input parameters given in Table 1. Round grey dots (150 in total) represent the modeled oceanic basalts; white-filled black squares and dots are the MORB and OIB data given in supplementary Table 1. Individual mantle end-member isotope compositions used in the modeling are shown in color.

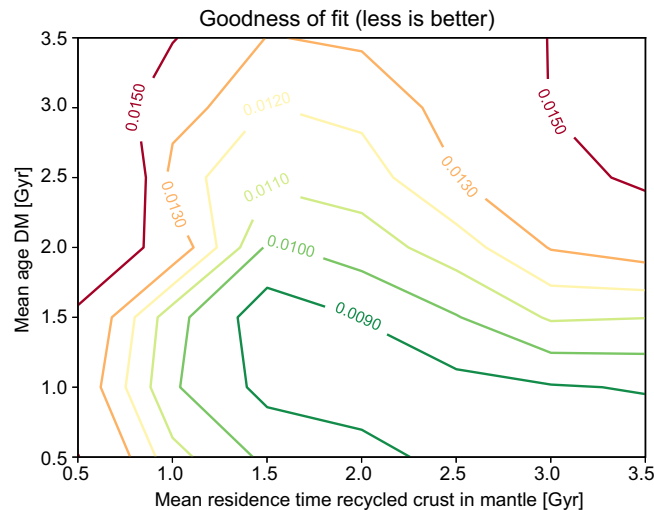


Fig. 6. The diagram shows (contoured) a goodness of fit after optimization for different values for the age of the depleted mantle (mean \pm 1S. D.) = $[0.5 \pm 0.25, 1 \pm 0.5, 1.5 \pm 0.75, 2 \pm 1, 2.5 \pm 1.25, 3 \pm 1.5, 3.5 \pm 1.75]$ and recycling time of enriched components in the mantle $[0.5 \pm 0.25, 1 \pm 0.5, 1.5 \pm 0.75, 2 \pm 1, 2.5 \pm 1.25, 3 \pm 1.5, 3.5 \pm 1.75]$. Free model parameters are the sampled OC/DM, sampled CC/OC, sampled LCC/(LCC + UCC), and the crustal storage time. The goodness of fit score is optimized using a gradient descent algorithm that minimizes the average squared distance between a model point and the closest data point (for details see supplementary material), using 60 modeled oceanic basalts for each model run.

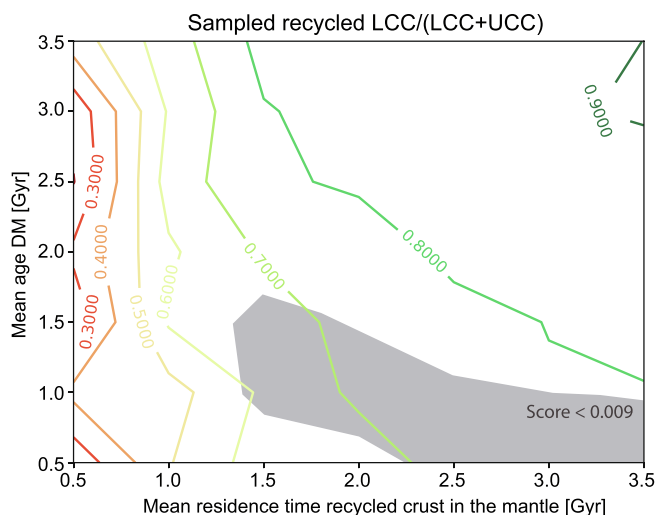


Fig. 7. The diagram shows optimized values for sampled LCC/(LCC + UCC) for different values for the age of the depleted mantle (mean \pm 1S.D.) = $[0.5 \pm 0.25, 1 \pm 0.5, 1.5 \pm 0.75, 2 \pm 1, 2.5 \pm 1.25, 3 \pm 1.5, 3.5 \pm 1.75]$ and recycling time of enriched components in the mantle $[0.5 \pm 0.25, 1 \pm 0.5, 1.5 \pm 0.75, 2 \pm 1, 2.5 \pm 1.25, 3 \pm 1.5, 3.5 \pm 1.75]$. Free parameters are the sampled OC/DM, sampled CC/OC, sampled LCC/(LCC + UCC), and the crustal storage time. The goodness of fit score is optimized using a gradient descent algorithm that minimizes the average squared distance between a model point and the closest data point (supplementary material), using 60 modeled oceanic basalts for each model run. Also shown in gray is the parameter area for which sufficiently good goodness of fit scores resulted in Fig. 6.

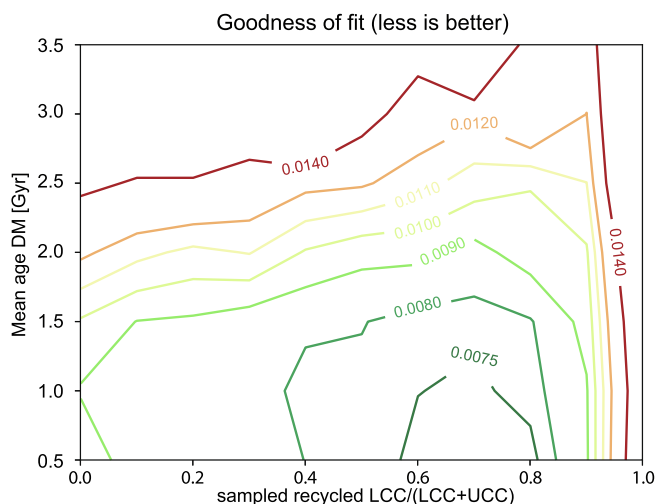


Fig. 8. The diagram shows a goodness of fit after optimization for different values for the age of the depleted mantle (mean \pm 1S.D.) = $[0.5 \pm 0.25, 1 \pm 0.5, 1.5 \pm 0.75, 2 \pm 1, 2.5 \pm 1.25, 3 \pm 1.5, 3.5 \pm 1.75]$ and the recycled LCC/(UCC + LCC) sampled by oceanic basalts = $[0 \pm 0, 0.1 \pm 0, 0.2 \pm 0, 0.3 \pm 0, 0.4 \pm 0, 0.5 \pm 0, 0.6 \pm 0, 0.7 \pm 0, 0.8 \pm 0, 0.9 \pm 0, 1 \pm 0]$. Free parameters are the sampled OC/DM, sampled CC/OC, crustal storage time, and the recycling time of crustal material in the mantle. The goodness of fit score is optimized using a gradient descent algorithm that minimizes the average squared distance between a model point and the closest data point (supplementary material), using 60 modeled oceanic basalts for each model run.

are contoured in Fig. 6. Best fit models have mean DM ages < 1.5 Ga and recycled crust ages > 1 Ga. Outside of these bounds, the model fits become increasingly poor; although admittedly the exact cut-off for scores that provide a good fit is somewhat subjective, and dependent on the selection of controlled parameters.

Several observations can be made with respect to the proportion of recycled LCC to total continental crust (LCC + UCC; Fig. 7). The optimal solutions, found on convergence with the gradient decent algorithm, have a rel-

atively high amount of recycled LCC in the melt relative to UCC (ca. 7/3, i.e., $LCC/(LCC + UCC) = 0.7$; Fig. 7). This fine-tuned proportion of LCC/(LCC + UCC) is a function of the crustal age and the age of the DM. In general, when longer recycling times are imposed on the optimization algorithm, higher LCC/(LCC + UCC) are required (Fig. 7). This effect arises because as the continental crust components become older and isotopically more extreme, less recycled UCC is required to reproduce the most isotopically enriched OIB (Fig. 4). In addition, older, isotopi-

cally more extreme DM leads to pronounced curvature in the mixing trends between DM and the recycled components (OC, LCC, UCC), and to mixing over a larger isotopic range, which offsets the mantle array towards higher ϵNd and ϵHf at given ϵCe . In part, the models compensate for this effect during optimization by increasing the ratios of LCC/(LCC + UCC) (Figs. 3, 4 and 7) and OC/DM (see [supplementary material](#)).

4.3.2. Age of the DM and defining LCC/UCC recycling ratios

Better constraints on the sampling of recycled LCC in oceanic basalts can be obtained if the ratio of LCC/(LCC + UCC) is a controlled variable (Fig. 8), which is systematically explored rather than a free parameter optimized by gradient descent (as done for Fig. 7). Optimized goodness of fit scores are mapped out in Fig. 8 as a function of the age of the DM and LCC/(LCC + UCC). Depleted mantle (DM) older than 1.5–2 Ga yields poor fits with the observed Ce–Nd–Hf mantle array, as in Fig. 6. Models devoid of recycled UCC (right side of the diagram) fail to replicate the mantle array. Good fits (score < 0.008) are attained for recycled LCC to UCC sampling ratios of 4:6 to 8:2 (i.e., LCC/(LCC + UCC) = 0.4–0.8).

5. DISCUSSION

5.1. Recycling oceanic crust (OC)

Recycled OC has a large influence on the slope of the modeled Ce–Nd–Hf array, because with age, the recycled bulk OC develops isotope ratios that increasingly deviate from the observed Ce–Hf and Nd–Hf array (Fig. 2). However, mixtures of melts from DM and recycled bulk OC in our model can only account for isotope ratios in the upper left quadrant in Figs. 2a,b, 3a,b and 4a,b; that is, $\epsilon\text{Nd} > 0$, $\epsilon\text{Hf} > 0$, and $\epsilon\text{Ce} < 0$. For reproducing isotope ratios that extend the observed isotopic variation to $\epsilon\text{Nd} < 0$, $\epsilon\text{Hf} \leq 0$, and $\epsilon\text{Ce} > 0$, the presence of recycled UCC or LCC is required. This effect makes it difficult to extract tight constraints on the age of the recycled OC. Nevertheless, for the recycled bulk OC and associated variance assumed, the best-fit models have mean ages > 1 Ga (and DM ages of < 1.5 Ga, Figs. 6 and 7). The residence time of recycled OC in the mantle therefore exceeds the turn-around time of the mantle, which is on the order of several 100 Myr for convective mantle velocities of cm/yr. Hence, the > 1 Ga residence time of OC implies that it is stored for considerable time in Earth's mantle before being reprocessed by partial melting in MORB and OIB sources.

The model results, however, depend strongly on the assumed composition of the recycled OC. We use bulk OC (White and Klein, 2014), which consists of the upper extrusive crust (MORB) and the lower oceanic gabbros, rather than solely MORB. To account for differences in bulk OC composition on a global scale, we assign compositional variance as described in Section 5.1. The limited data for the lower OC (i.e., gabbros) show that it is highly heterogeneous on a local and global scale (e.g., Coogan, 2014; White and Klein, 2014; Fig. 9). This limited knowl-

edge about the average composition of the lower OC, in addition to large variability of MORB (Arevalo and McDonough, 2010; Jenner and O'Neill, 2012; Gale et al., 2013; White and Klein, 2014; Yang et al., 2018), imposes considerable uncertainty on the average composition and variability of the bulk recycled OC (e.g., Stracke et al., 2003; White and Klein, 2014). Hence, it is difficult to judge whether the model input parameter, the bulk OC of White and Klein (2014), under- or overestimates the natural variance.

For evaluating the uncertainty associated with the recycled bulk OC it is important to consider that the OC is compositionally heterogeneous on different scales. On a local scale, e.g., the scale of ridge segments, compositional variability is caused by differences in mantle composition and extent of mantle melting due to variable mantle temperature. At the scale of an individual cross section of OC, the upper OC (i.e., MORB) differs from the lower crustal gabbros, mostly due to fractional crystallization (e.g., Coogan, 2014). If the compositional heterogeneity within the bulk OC, that is, the upper and lower OC together, is preserved during recycling, residence in the mantle, and subsequent sampling by oceanic volcanism, ancient OC develops considerable isotopic heterogeneity (e.g., Chauvel and Hémond, 2000; Koornneef et al., 2012; Stracke et al., 2003, 2005). The expected range of isotope ratios of recycled 2 Ga upper MORB alone, for example, covers the entire Ce–Nd–Hf mantle array (Fig. 9). In principal, therefore, a large part of the mantle array might be explained solely by recycling MORB if its entire compositional variability is considered.

However, the region in Fig. 9 where ancient recycled MORB plot most densely is offset from the mantle array towards lower $^{138}\text{Ce}/^{136}\text{Ce}$. Moreover, the observed mantle array in Ce–Nd–Hf isotopic space is very narrow, which is difficult to maintain if the entire range of observed MORB compositions would be sampled with equal probability, given the large isotopic variance of recycled MORB perpendicular to the observed Ce–Nd–Hf mantle array (Fig. 9). A moderating element is thus required to shift recycled MORB towards the observed Ce–Nd–Hf mantle array. This is achieved by the additional presence of lower oceanic gabbros, which develop lower ϵCe , but higher ϵNd and ϵHf compared to recycled MORB (Fig. 9).

Consequently, considering that recycled OC is not just MORB, but rather a package of upper and lower OC (i.e., MORB + gabbros), the isotope ratios of bulk recycled OC fall closer to the observed Ce–Nd–Hf mantle array. Moreover, because the observed Ce–Nd–Hf mantle array is very narrow (Fig. 1), it is apparent that not the entire compositional variance of the recycled OC is transferred into oceanic basalt sources. This is plausible, because many sources of internal chemical variance average out on the scale of the bulk OC, and during subsequent sampling of recycled OC by partial melting. Thus, the geochemical variance between subducting packages of bulk OC is expected to be less than the internal variance within each lithological unit (MORB vs. gabbros). In addition, the predicted global variance of recycled OC is likely reduced by stirring and mingling during subduction and mantle processing, and

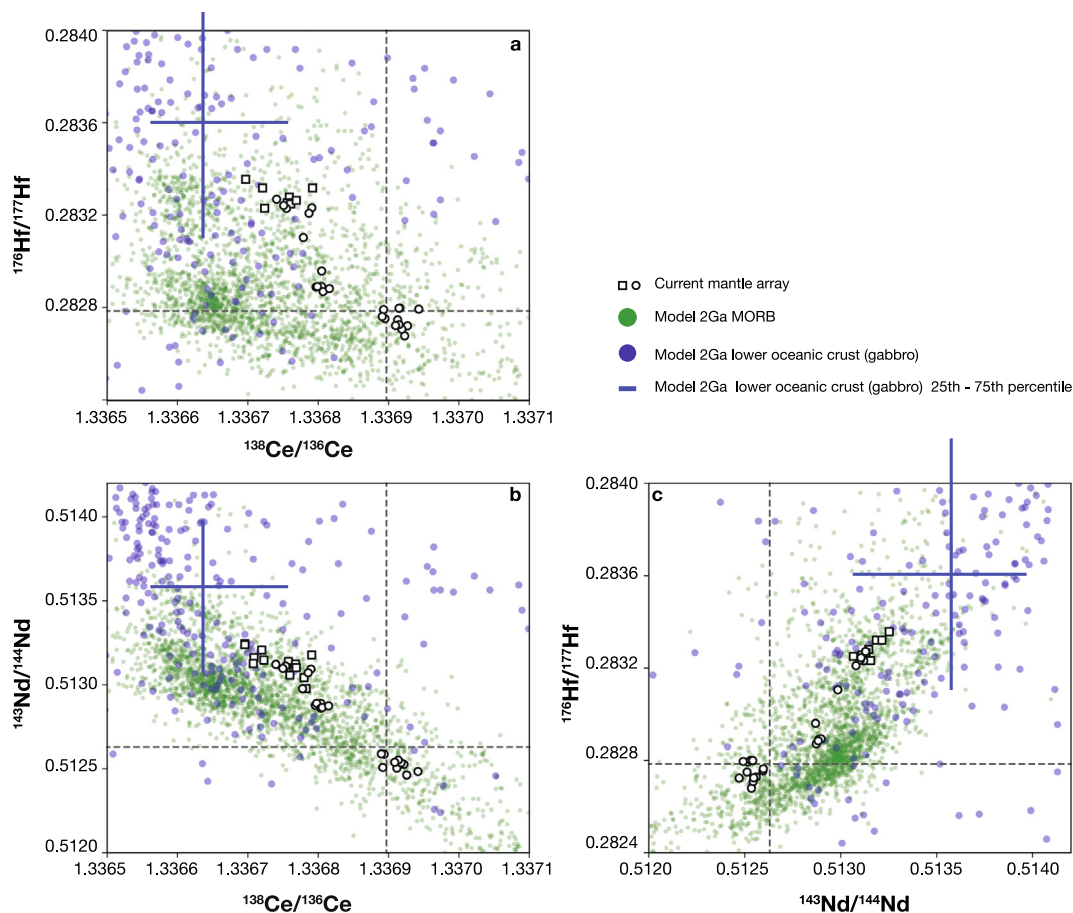


Fig. 9. Diagrams of (a) $^{176}\text{Hf}/^{177}\text{Hf}$ versus $^{138}\text{Ce}/^{136}\text{Ce}$, (b) $^{143}\text{Nd}/^{144}\text{Nd}$ versus $^{138}\text{Ce}/^{136}\text{Ce}$, and (c) $^{176}\text{Hf}/^{177}\text{Hf}$ versus $^{143}\text{Nd}/^{144}\text{Nd}$ show the isotopic distribution of 2 Ga MORB (green) and lower oceanic crustal gabbro (blue). The modeled MORB ($n = 2459$) and gabbro ($n = 286$) isotope ratios are obtained by isotopic evolution from DM at 2 Ga (Section 5.2) using the La/Ce, Sm/Nd and Lu/Hf from the MORB compilation by Gale et al. (2013), and Gabbro trace element data obtained from the PetDB (supplementary Table 3). The large compositional variability of MORB (and gabbro) results in a large range of isotope compositions that covers the entire Ce-Nd-Hf mantle array (white-filled black squares: MORB, white-filled black dots: OIB).

subsequently, during partial melting of heterogeneous mantle sources by oceanic volcanism.

Hence, for evaluating the influence of recycled OC on mantle evolution it is crucial to consider the composition of the bulk OC, rather than only the extrusive basalts, i.e. MORB (cf. Stracke et al., 2003). Nevertheless, the composition and variance of recycled bulk OC remains a major unknown; not only in our model, but also for our general understanding of global geochemical fluxes between the crust and mantle.

5.2. Recycling of continental crust

Although recycling OC can produce a large range of isotope ratios, the majority concentrates at $\epsilon\text{Nd} > 0$, $\epsilon\text{Hf} \geq 0$, and $\epsilon\text{Ce} < 0$ (Fig. 9). Oceanic basalts with $\epsilon\text{Nd} < 0$, $\epsilon\text{Hf} \leq 0$, and $\epsilon\text{Ce} > 0$ thus require at least one additional, incompatible element enriched, high ϵCe but low ϵNd - ϵHf source component, that is, a continental crust component. Even though the compositional variability of the recycled bulk OC might be larger than accounted for by the compo-

sition in our model (White and Klein, 2014, see discussion above), this conclusion appears robust. Chauvel et al. (2008) reached a similar conclusion on basis of the global distribution of Nd-Hf isotope ratios in oceanic basalts, which is re-affirmed by the Ce-Hf and Nd-Hf isotope systematics modeled here.

Note that the tolerable amount of sediment in the mantle source for successful model solutions (Figs. 6–8) is on the order of a few percent or less, which is in good agreement with inferences from previous studies (e.g., Chauvel et al., 1992; Stracke et al., 2003; Wright and White, 1987). The parameters for one exemplary model solution are given in Table 2 and illustrated in Fig. 5. For this example, the mantle source OC/DM is 0.19, and the CC/OC is 0.07, that is, the mantle source consists of ca. 83% DM, 16% OC, and 1% continental crust (of which ca. 70% is LCC and the rest UCC). Considerably larger amounts of sediment create Ce-Nd-Hf isotope ratios closer to those of the LCC and UCC end-members (Fig. 2), that is, would extend the modeled Ce-Nd-Hf mantle array beyond the observed range of values. This effect would result in a low goodness of fit score,

and such parameter combinations are therefore not included in the model solutions discussed here (Figs. 6–8).

In Ce-Nd and Ce-Hf isotope space, LCC and UCC vectors are more divergent than in Nd-Hf isotope space (Fig. 2). Thus, considering Ce in addition to Nd-Hf isotope ratios provides valuable additional constraints on the type of recycled continental crust. The sensitivity of the Ce isotope system to the ratio of LCC/UCC sampled in oceanic basalts has a significant impact on the extent and slope of the modeled Ce-Nd-Hf mantle array (Fig. 2). Good model fits result for LCC/UCC = 4/6 to 8/2 (i.e., LCC/(UCC + LCC) = 0.4–0.8; Fig. 8), consistent with the high proportion of recycled LCC suggested from Fig. 6. While this range is relatively broad, it does suggest that the majority of the continental crustal return flux into Earth's mantle is from the LCC (e.g., Willbold and Stracke, 2006, 2010), which is consistent with recent models for developing and maintaining an average andesitic composition of the continental crust (Kelemen et al., 2014; Rudnick and Gao, 2014).

5.3. Age of the depleted mantle

The best-fit DM ages inferred from our model (Figs. 6–8) have mean depletion ages between 0.5 Ga (± 0.25 , 1 S.D.) to 1.5 Ga (± 0.75 , 1 S.D.). This range of depletion ages is similar to Sm-Nd model ages of abyssal peridotites, which are generally < 1 Ga, but with sporadic ages up to 2.7 Ga (Cipriani et al., 2004; Warren et al., 2009; Stracke et al., 2011; Mallick et al., 2014; Brunelli et al., 2018). Rhenium-Os model ages (T_{RD}) in abyssal peridotites have a similar distribution (e.g., Alard et al., 2005; Brandon et al., 2000; Day et al., 2017; Harvey et al., 2006; Lassiter et al., 2014; Liu et al., 2008; Snow and Reisberg, 1995; Standish et al., 2002; Warren et al., 2009), with an average of 0.77 Ga ± 0.93 (2 S.D.) (Day et al., 2017). The Sm-Nd and Re-Os (T_{RD}) model ages of abyssal peridotites are thus consistent with the young DM ages inferred from our model (Figs. 6–8). Nevertheless, both the sporadic > 2 Ga Sm-Nd and Re-Os model ages, or the apparent preservation of mass independent sulfur isotope signatures in mantle sulfides (Cabral et al., 2013), potentially suggest that the memory of such old events is not completely erased. However, the signatures observed in elements with very different geochemical behavior (the REE Nd, and the variably siderophile and chalcophile elements Os and S) reflect a range of processes that are not necessarily interrelated.

The young DM ages inferred from our model (Figs. 6–8) rely on the assumption that the existing DM estimates used for the modeling (Salters and Stracke, 2004; Workman and Hart, 2005) accurately capture the average composition of the DM. As discussed below (Section 5.4), these estimates are expected to somewhat underestimate the average incompatible element depletion of the DM. Using a more incompatible element depleted DM end-member, the model presented here yields younger, less variable ages for the DM. The best-fit age for the DM (<1.5 Ga, Figs. 5–7) with the parameters used in our model (Salters and Stracke, 2004; Workman and Hart, 2005) should thus be considered an upper bound.

If the depletion ages inferred from our model (<1.5 Ga) reflect the time of the last melting event the mantle has experienced, they constrain the rate of mantle processing through melting regions in the shallow mantle. This so-called mantle processing rate is proportional to the mass fraction of mantle that has become depleted by partial melting and the number of melting events experienced by its individual parts. The mantle processing rate therefore determines the present extent of mantle depletion, and is a proxy for the overall rate of silicate earth differentiation (e.g., Stracke, 2018; Tackley, 2015). Hence, if the young DM ages of our model indicate that the mantle re-melts within < 1.5 Ga, which is consistent with the ~ 1.2 Ga estimated based on Os isotope ratios in abyssal peridotites (Chatterjee and Lassiter, 2016), the processing rate of the mantle would be considerably faster than inferred from oceanic crust production rates (e.g., Stracke, 2018; Stracke et al., 2003; Tackley, 2015). If so, the resulting large extent of mantle depletion must be counteracted, on a global scale, by a relatively large return flux of subducted oceanic and continental crust.

5.4. The nature of the depleted mantle

If the fast mantle processing rate inferred from our modeled DM ages is correct, most of Earth's mantle should have experienced more than one melting event over Earth's history, and should thus be highly depleted. Mixing arrays with melts from highly depleted mantle and incompatible element enriched sources (OC, UCC, LCC), however, have a pronounced curvature (Fig. 3). On a global scale, this scenario would produce a Ce-Nd-Hf mantle array with a steeper slope than observed (Fig. 3, cf. Willig and Stracke, 2019). Apparently therefore, a DM with moderate isotopic, and thus time-integrated average incompatible element depletion is required to reproduce the Ce-Nd-Hf mantle array (Figs. 3 and 4).

For evaluating the composition of the average DM involved in our model it must be considered that DM is intrinsically heterogeneous. Generating DM by partial melting at mid ocean ridges, for example, strongly depletes the mantle by high degree melting under the ridge axis, but only slightly depletes the mantle by low degree melting off-axis (Langmuir et al., 1992; Fig. 10). Strongly incompatible elements ($D < 0.01$) are quantitatively extracted at low degrees (≤ 3 –5%) of melting and thus retain significant concentrations only in the lower parts of the residual mantle, i.e., those that have experienced the smallest degree of melting (Fig. 10). Formation of DM therefore invariably produces a range of intrinsically heterogeneous mantle materials.

Incompatible element abundances and ratios in aggregate melts from a heterogeneous DM, including isotope ratios of the lithophile radiogenic isotope systems (Sm-Nd, Rb-Sr, Pb-U, Th-U, and here La-Ce), thus reflect the average incompatible element inventory of a range of highly to slightly incompatible element depleted materials. However, although highly depleted materials constitute most of the DM (Fig. 10), they contain only small amounts of incompatible elements (e.g., Ce, Nd, Hf). The total

incompatible element inventory of a heterogeneous DM is thus dominated by its least depleted parts. Incompatible element ratios (and concentrations) of this average DM are therefore similar to the more moderately depleted materials of the underlying spectrum of variably depleted mantle. The average La/Ce for the residual mantle shown in Fig. 10, for example, is $0.63 \times \text{La}/\text{Ce}_0$, where La/Ce_0 is the La/Ce of the mantle before partial melting. This apparent La/Ce corresponds to the residual mantle produced by 1.6% single-stage fractional melting, compared to the average of 6% for the example shown in Fig. 10. Hence, if the apparent moderate extent of depletion reflected in melts from a heterogeneous DM is taken to reflect bulk source composition, rather than the average of a range of heterogeneous materials, the extent of melt extraction and incompatible element depletion of the DM source is underestimated.

Consequently, the apparent moderate depletion of the DM indicated by our model is deceiving, because the moderately depleted melts required to reproduce the slope of the Ce-Nd-Hf reflect a biased average of an intrinsically heterogeneous DM, rather than a moderately incompatible element depleted and compositionally homogeneous DM. The total compositional range of DM involved in generating the observed Ce-Nd-Hf mantle array is therefore probably larger than inferred from our model.

Note that underestimating the extent of depletion and compositional variability of DM from incompatible ele-

ment and isotope ratios in MORB also presents an obstacle for estimating DM composition (Salters and Stracke, 2004; Workman and Hart, 2005), and for inferring the correct extent of depletion and mass of DM from geochemical and isotopic mass balance (e.g., Allègre et al., 1979; Hofmann, 1986).

6. CONCLUSIONS

Cerium isotope ratios, in addition to the conventional lithophile Nd-Hf (and Sr-Pb) isotope ratios are a unique tool for identifying the role of variably depleted mantle in MORB and OIB generation, and provide valuable constraints on the nature of recycled oceanic and continental crust (i.e., upper vs. lower continental crust) components in Earth's mantle.

The combined Ce-Nd-Hf isotope ratios, for example, provide better constraints on the nature and abundance of DM in MORB and OIB sources. On a local scale, the pronounced curvature of mixing arrays towards different DM components can identify variably depleted mantle sources (Figs. 3 and 4). The slope and dispersion of the observed Ce-Nd-Hf mantle array are also heavily influenced by the average DM involved in MORB and OIB generation (Figs. 2–5). Reproducing the slope of the observed Ce-Nd-Hf mantle array by repeated sampling of an underlying variable population of mantle components (DM, recycled OC, UCC, LCC) in a “Monte Carlo”

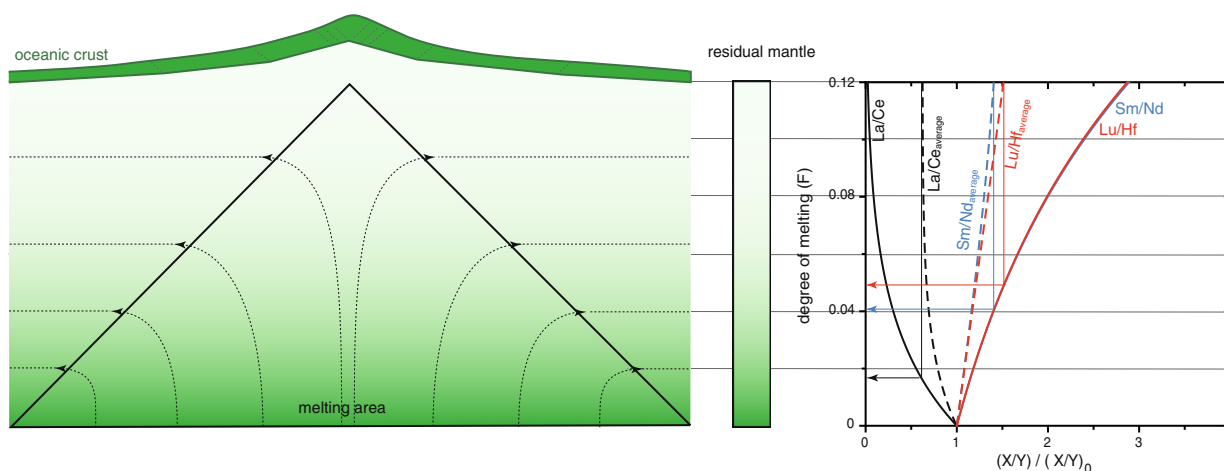


Fig. 10. The diagram on the left shows a schematic triangular melting area beneath a mid ocean ridge, assuming a maximum extent of melting of 12% directly underneath the ridge axis. Assuming that incompatible elements are completely exhausted after 5% of melting (i.e., at about half the height) 58% of the mantle that returns into the deeper mantle is highly depleted (for exhaustion of incompatible elements at 3% of melting, it becomes ca. 75%). Effectively, this means that highly depleted mantle, almost devoid of incompatible elements is the volumetrically dominant component of depleted mantle. The diagram on the right shows how the La/Ce, Sm/Nd and Lu/Hf ratios change from bottom to top of the residual mantle, i.e., with increasing degree of melting. La/Ce decreases from $\text{La}/\text{Ce} \sim 0.97 \times \text{La}/\text{Ce}_0$ (where La/Ce_0 is the La/Ce of the unmelted mantle) in the lower part of the residual mantle (0.1% melt) to $\text{La}/\text{Ce} \sim 0.02 \times \text{La}/\text{Ce}_0$ in the upper part of the residual mantle (12% melt, black line). For a uniform distribution of the degree of melt in the residual mantle from 0.1–12%, the average La/Ce for the residual mantle is $\sim 0.63 \times \text{La}/\text{Ce}_0$ (black dashed line). This average extent of depletion corresponds to the residue of 1.6% single-stage fractional melting, rather than the actual 6% produced. Sm and Nd are more compatible and yield average Sm/Nd of $1.40 \times \text{Sm}/\text{Nd}_0$ corresponding to $\sim 4\%$ melt depletion (blue lines). For Lu/Hf, the average is $1.51 \times \text{Lu}/\text{Hf}_0$ corresponding to $\sim 4.9\%$ fractional melting (red lines). Hence, the average of a heterogeneous DM is increasingly biased towards the least depleted DM components for increasingly more incompatible elements ratios. This bias is transposed to partial melts, i.e., incompatible element ratios in partial melts from a heterogeneous DM are biased towards the least depleted parts of the DM. Bulk partition coefficients for melting of spinel peridotite are $D_{\text{La}} = 0.013$, $D_{\text{Ce}} = 0.021$, $D_{\text{Nd}} = 0.046$, $D_{\text{Sm}} = 0.075$, $D_{\text{Hf}} = 0.073$, $D_{\text{Lu}} = 0.186$ (Stracke and Bourdon, 2009).

approach requires melts from average DM that are only moderately depleted. However, because these melts do not reflect melting of a single homogeneous DM, but rather the total incompatible element inventory of a much greater range of inherently heterogeneous DM, the extent of depletion and variability of the DM is larger than indicated by the modeled melts.

Our model results further show that it is crucial to consider the composition of recycled bulk OC, i.e., both the extrusive basalts and intrusive gabbroic rocks of the lower oceanic crust, for evaluating the role recycled OC on mantle compositions and crust-mantle cycling in general (cf. [Stracke et al., 2003](#)). The low dispersion of the observed Ce-Nd-Hf mantle array suggests that the total compositional variance of the oceanic crust is not reflected in MORB and OIB sources. One reason for this effect is that individual variability averages out on the scale of the bulk oceanic crust, and during subsequent sampling of recycled oceanic crust by partial melting. Another reason is that the ubiquitous presence of recycled continental crust, which is required to account for the full range of Ce-Nd-Hf isotope ratios in oceanic basalts (cf. [Chauvel et al., 2008](#)), masks the signatures of recycled oceanic crust. Nevertheless, uncertainties in bulk composition of recycled oceanic crust are a major source of uncertainty for evaluating the isotopic evolution of Earth's mantle, and crust mantle cycling in general, especially considering that subducted oceanic crust is by far the greatest mass flux into the mantle.

Owing to the distinct LREE patterns of upper and lower continental crust, combined Ce-Nd-Hf systematics can also distinguish between different recycled continental crust components in MORB and OIB sources, on both local and global scale. Our model result indicate that the return flux from the continental crustal into Earth's mantle derives to a large extent from the lower continental crust (e.g., [Willbold and Stracke, 2006, 2010](#)), consistent with recent models for developing and maintaining an average andesitic composition of the continental crust ([Kelemen et al., 2014; Rudnick and Gao, 2014](#)).

Overall, therefore, Ce in addition to other lithophile isotope ratios (Sr-Nd-Hf-Pb) provide valuable constraints on the nature of MORB and OIB source components, on crust-mantle exchange, and silicate Earth evolution in general.

Declaration of Competing Interest

The authors declare that they have no known competing financial interests or personal relationships that could have appeared to influence the work reported in this paper.

ACKNOWLEDGMENTS

The authors thank John Lassiter, Bill White and an anonymous reviewer for their constructive comments, which considerably improved the clarity and presentation of the manuscript. Jeff Catalano is thanked for his efficient, pragmatic editorial handling. This work was supported by the German Research Foundation (DFG) through grant STR853/5-1. The National High Magnetic Field Laboratory is supported by the National Science Foundation through NSF/DMR-1157490 and the State of Florida.

We thank Heidi Baier for technical assistance and are grateful for discussions with Erik Scherer.

APPENDIX A. SUPPLEMENTARY MATERIAL

Supplementary data to this article can be found online at <https://doi.org/10.1016/j.gca.2019.12.029>.

REFERENCES

- Alard O., Luguet A., Pearson N. J., Griffin W. L., Lorand J.-P., Gannoun A., Burton K. W. and O'Reilly S. Y. (2005) In situ Os isotopes in abyssal peridotites bridge the isotopic gap between MORBs and their source mantle. *Nature* **436**, 1005–1008.
- Allègre C. J. (1982) Chemical geodynamics. *Tectonophys.* **81**, 109–132.
- Allègre C. J., Ben Othman D., Polve M. and Richard P. (1979) The Nd-Sr isotopic correlation in mantle materials and geodynamic consequences. *Phys. Earth Planet. Int.* **19**, 293–306.
- Arevalo R. and McDonough W. F. (2010) Chemical variations and regional diversity observed in MORB. *Chem. Geol.* **271**, 70–85.
- Begemann F., Ludwig K. R., Lugmair G. W., Min K., Nyquist L. E., Patchett P. J., Renne P. R., Shih C. Y., Villa I. M. and Walker R. J. (2001) Call for an improved set of decay constants for geochronological use. *Geochim. Cosmochim. Acta* **65**, 111–121.
- Bellot N., Boyet M., Doucelance R., Pin C., Chauvel C. and Auclair D. (2015) Ce isotope systematics of island arc lavas from the Lesser Antilles. *Geochim. Cosmochim. Acta* **168**, 261–279.
- Blichert-Toft J., Gleason J. D., Telouk P. and Albarede F. (1999) The Lu-Hf isotope geochemistry of shergottites and the evolution of the Martian mantle-crust system. *Earth Planet. Sci. Lett.* **173**, 25–39.
- Bouvier A., Vervoort J. D. and Patchett P. J. (2008) The Lu-Hf and Sm-Nd isotopic composition of CHUR: Constraints from unequilibrated chondrites and implications for the bulk composition of terrestrial planets. *Earth Planet. Sci. Lett.* **273**, 48–57.
- Boyet M., Doucelance R., Israel C., Bonnand P., Auclair D., Suchorski K. and Bosq C. (2019) New constraints on the origin of the EM-1 component revealed by the measurement of the La-Ce isotope systematics in Gough Island lavas. *Geochim. Geophys. Geosys.* **20**, 2484–2498, doi:10.1029/2019GC008228.
- Brandon A. D., Snow J. E., Walker R. J., Morgan J. W. and Mock T. D. (2000) 190Pt-186Os and 187Re-187Os systematics of abyssal peridotites. *Earth Planet. Sci. Lett.* **177**, 319–335.
- Brunelli D., Cipriani A. and Bonatti E. (2018) Thermal effects of pyroxenites on mantle melting below mid-ocean ridges. *Nat. Geosci.* **11**, 520–525.
- Brunelli D., Paganelli E. and Seyler M. (2014) Percolation of enriched melts during incremental open-system melting in the spinel field: A REE approach to abyssal peridotites from the Southwest Indian Ridge. *Geochim. Cosmochim. Acta* **127**, 190–203.
- Brunelli D., Seyler M., Cipriani A., Ottolini L. and Bonatti E. (2006) Discontinuous melt extraction and weak refertilization of mantle peridotites at the vema lithospheric section (mid-Atlantic ridge). *J. Petrol.* **47**, 745–771.
- Cabral R. A., Jackson M. G., Rose-Koga E. F., Koga K. T., Whitehouse M. J., Antonelli M. A., Farquhar J., Day J. M. D. and Hauri E. H. (2013) Anomalous sulphur isotopes in plume lavas reveal deep mantle storage of Archaean crust. *Nature* **496**, 490–493.

- Chatterjee R. and Lassiter J. C. (2016) 186Os/188Os variations in upper mantle peridotites: Constraints on the Pt/Os ratio of primitive upper mantle, and implications for late veneer accretion and mantle mixing timescales. *Chem. Geol.* **442**, 11–22.
- Chauvel C. and Hémond C. (2000) Melting of a complete section of recycled crust oceanic crust: Trace element and Pb isotopic evidence from Iceland. *Geochem. Geophys. Geosys.* **1**, 1001, doi:10.1029/1999GC000002.
- Chauvel C., Hofmann A. W. and Vidal P. (1992) HIMU-EM: the French-Polynesian connection. *Earth Planet. Sci. Lett.* **110**, 99–119.
- Chauvel C., Lewin E., Carpentier M., Arndt N. T. and Marini J.-C. (2008) Role of recycled oceanic basalt and sediment in generating the Hf-Nd mantle array. *Nat. Geosc.* **1**, 64–67.
- Cipriani A., Brueckner H. K., Bonatti E. and Brunelli D. (2004) Oceanic crust generated by elusive parents: Sr and Nd isotopes in basalt-peridotite pairs from the Mid-Atlantic ridge. *Geology* **32**, 657–660.
- Coogan L. A. (2014) 4.14 - The Lower Oceanic Crust. In *Treatise on Geochemistry (Second Edition)* (eds. H. D. Holland and K. K. Turekian). Elsevier, Oxford, pp. 497–541.
- Day J. M. D., Walker R. J. and Warren J. M. (2017) 186Os–187Os and highly siderophile element abundance systematics of the mantle revealed by abyssal peridotites and Os-rich alloys. *Geochim. Cosmochim. Acta* **200**, 232–254.
- DePaolo D. J. (1980) Crustal growth and mantle evolution: inferences from models of element transport and Nd and Sr isotopes. *Geochim. Cosmochim. Acta* **44**, 1185–1196.
- Dickin A. (1988) Mantle and crustal Ce/Nd isotope systematics. *Nature* **333**, 403.
- Dickin A. P. (1987) Cerium isotope geochemistry of ocean island basalts. *Nature* **326**, 283–284.
- Gale A., Dalton C. A., Langmuir C. H., Su Y. and Schilling J.-G. (2013) The mean composition of ocean ridge basalts. *Geochem. Geophys. Geosys.* **14**, 489–518, doi:10.1029/2012GC004334.
- Harvey J., Gannoun A., Burton K. W., Rogers N. W., Alard O. and Parkinson I. J. (2006) Ancient melt extraction from the oceanic upper mantle revealed by Re-Os isotopes in abyssal peridotites from the Mid-Atlantic ridge. *Earth Planet. Sci. Lett.* **244**, 606–621.
- Hellebrand E. and Snow J. E. (2003) Deep melting and sodic metasomatism underneath the highly oblique-spreading Lena Trough (Arctic Ocean). *Earth Planet. Sci. Lett.* **216**, 283–299.
- Hofmann A. W. (1986) Nb in Hawaiian magmas - constraints on source composition and evolution. *Chem. Geol.* **57**, 17–30.
- Hofmann A. W. (1988) Chemical differentiation of the Earth - the relationship between mantle, continental-crust, and oceanic-crust. *Earth Planet. Sci. Lett.* **90**, 297–314.
- Hofmann A. W. (1997) Mantle geochemistry: The message from oceanic volcanism. *Nature* **385**, 219–229.
- Isobe T., Feigelson E. D., Akritas M. G. and Babu G. J. (1990) Linear regression in astronomy I. *Astrophys. J.* **364**, 104–113.
- Jacobsen S. B. and Wasserburg G. J. (1979) Mean age of mantle and crustal reservoirs. *J. Geophys. Res.* **84**, 7411–7427.
- Jenner F. E. and O'Neill H. S. C. (2012) Analysis of 60 elements in 616 ocean floor basaltic glasses. *Geochem. Geophys. Geosys.* **13**, Q02005, doi: 10.1029/2011gc004009.
- Kelemen P. B., Hanghøj K. and Greene A. R. (2014) 4.21 - One View of the Geochemistry of Subduction-Related Magmatic Arcs, with an Emphasis on Primitive Andesite and Lower Crust. In *Treatise on Geochemistry (Second Edition)* (eds. H. D. Holland and K. K. Turekian). Elsevier, Oxford, pp. 749–806.
- Koornneef J. M., Stracke A., Bourdon B., Meier M. A., Jochum K. P., Stoll B. and Grönvold K. (2012) Melting of a two-component source beneath Iceland. *J. Petrol.* **53**, 127–157.
- Kumari S., Paul D. and Stracke A. (2016) Open system models of isotopic evolution in Earth's silicate reservoirs: implications for crustal growth and mantle heterogeneity. *Geochim. Cosmochim. Acta* **195**, 142–157.
- Lambart S., Baker M. B. and Stolper E. M. (2016) The role of pyroxenite in basalt genesis: Melt-PX, a melting parameterization for mantle pyroxenites between 0.9 and 5 GPa. *J. Geophys. Res. Solid Earth* **121**, doi:10.1002/2015JB012762.
- Langmuir, C. H., Klein, E. M. and Plank, T. (1992) Petrological systematics of mid-ocean ridge basalts: constraints on melt generation beneath ocean ridges. In: Morgan, J.P., Blackman, D.K., Sinton, J.M. (Eds.). AGU, Washington, D C, pp. 183–210.
- Lassiter J. C., Byerly B. L., Snow J. E. and Hellebrand E. (2014) Constraints from Os-isotope variations on the origin of Lena Trough abyssal peridotites and implications for the composition and evolution of the depleted upper mantle. *Earth Planet. Sci. Lett.* **403**, 178–187.
- Liu C. Z., Snow J. E., Hellebrand E., Brüggemann G., von der Handt A., Büchl A. and Hofmann A. W. (2008) Ancient, highly depleted heterogeneous mantle beneath Gakkel ridge, Arctic ocean. *Nature* **452**, 311–316.
- Makishima A. and Masuda A. (1994) Ce isotope ratios of N-type MORB. *Chem. Geol.* **118**, 1–8.
- Mallick S., Dick H. J. B., Sachi-Kocher A. and Salters V. J. M. (2014) Isotope and trace element insights into heterogeneity of subridge mantle. *Geochem. Geophys. Geosys.* **15**, 2438–2453, doi:10.1002/2014GC005314.
- O'Nions R. K., Evensen N. M. and Hamilton P. J. (1979) Geochemical modeling of mantle differentiation and crustal growth. *J. Geophys. Res.* **84**, 6091–6101.
- Pertermann M. and Hirschmann M. M. (2003) Partial melting experiments on a MORB-like pyroxenite between 2 and 3GPa: Constraints on the presence of pyroxenite in basalt source regions from solidus location and melting rate. *J. Geophys. Res.* **108**, 215, doi:10.1029/2000JB000118.
- Plank T. (2014) 4.17 - The Chemical Composition of Subducting Sediments. In *Treatise on Geochemistry (Second Edition)* (ed. H. D. H. K. Turekian). Elsevier, Oxford, pp. 607–629.
- Rudnick R. L. and Gao S. (2014) 4.1 - Composition of the Continental Crust. In *Treatise on Geochemistry (Second Edition)* (ed. H. D. H. K. Turekian). Elsevier, Oxford, pp. 1–51.
- Salters V. J. M. and Dick H. J. B. (2002) Mineralogy of the mid-ocean-ridge basalt source from neodymium isotopic composition of abyssal peridotites. *Nature* **418**, 68–72.
- Salters V. J. M., Mallick S., Hart S. R., Langmuir C. H. and Stracke A. (2011) Domains of depleted mantle; new evidence from hafnium and neodymium isotopes. *Geochem. Geophys. Geosys.* **12**, Q10017, doi:10.1029/2011GC003874.
- Salters V. J. M. and Stracke A. (2004) Composition of the depleted mantle Q05B07. *Geochem. Geophys. Geosys.* **5**, doi:10.1029/2003GC000597.
- Salters V. J. M. and White W. M. (1998) Hf isotope constraints on mantle evolution. *Chem. Geol.* **145**, 447–460.
- Sanfilippo A., Salters V., Tribuzio R. and Zanetti A. (2019) Role of ancient, ultra-depleted mantle in Mid-Ocean-Ridge magmatism. *Earth Planet. Sci. Lett.* **511**, 89–98.
- Sato J. and Hirose T. (1981) Half-life of ¹³⁸La. *Radiochem. Radioanal. Lett.* **46**, 145–152.

- Snow J. E. and Reisberg L. (1995) Os isotopic systematics of the MORB mantle - results from altered abyssal peridotites. *Earth Planet. Sci. Lett.* **133**, 411–421.
- Sobolev A. V., Hofmann A. W., Kuzmin D. V., Yaxley G. M., Arndt N. T., Chung S.-L., Danyushevsky L. V., Elliott T., Frey F. A., Garcia M. O., Gurenko A. A., Kamenetsky V. S., Kerr A. C., Krivolutsкая N. A., Matvienkov V. V., Nikogosian I. K., Rocholl A., Sigurdsson I. A., Sushchevskaya N. M. and Teklay M. (2007) The amount of recycled crust in sources of mantle-derived melts. *Science* **316**, 412.
- Standish J. J., Hart S. R., Blusztjan J., Dick H. J. B. and Lee K. L. (2002) Abyssal peridotite osmium isotopic compositions from Cr-spinel. *Geochem. Geophys. Geosyst.* **3**, 1004, doi:10.1029/2001GC000161.
- Stracke A. (2012) Earth's heterogeneous mantle: A product of convection-driven interaction between crust and mantle. *Chem. Geol.* **330–331**, 274–299.
- Stracke A. (2016) Depleted Mantle. In *Encyclopedia of Marine Geosciences* (eds. J. Harff, M. Meschede, S. Petersen and J. Thiede). Springer, Netherlands, pp. 182–185.
- Stracke A. (2018) Mantle Geochemistry. In *Encyclopedia of Geochemistry: A Comprehensive Reference Source on the Chemistry of the Earth* (ed. W. M. White). Springer International Publishing, Cham.
- Stracke A., Bizimis M. and Salters V. J. M. (2003) Recycling of oceanic crust: quantitative constraints. *Geochem. Geophys. Geosyst.* **4**, 8003, doi: 8010.1029/2001GC000223.
- Stracke A. and Bourdon B. (2009) The importance of melt extraction for tracing mantle heterogeneity. *Geochim. Cosmochim. Acta* **73**, 218–238.
- Stracke A., Genske F., Berndt J. and Koornneef J. M. (2019) Ubiquitous ultra-depleted domains in Earth's mantle. *Nat. Geosci.* **12**, 851–855.
- Stracke A., Hofmann A. W. and Hart S. R. (2005) FOZO, HIMU and the rest of the mantle zoo. *Geochem. Geophys. Geosyst.* **6**, Q05007, doi: 05010.01029/02004GC000824.
- Stracke A., Snow J. E., Hellebrand E., von der Handt A., Bourdon B., Birbaum K. and Günther D. (2011) Abyssal peridotite Hf isotopes identify extreme mantle depletion. *Earth Planet. Sci. Lett.* **308**, 359–368.
- Tackley P. J. (2015) 7.12 - Mantle Geochemical Geodynamics. In *Treatise on Geophysics* (ed. G. Schubert). Elsevier, Oxford, pp. 521–585.
- Tanaka T., Shimizu H., Kawata Y. and Masuda A. (1987) Combined La-Ce and Sm-Nd isotope systematics in petrogenetic studies. *Nature* **327**, 113–117.
- Vervoort J. D. and Patchett P. J. (1996) Behavior of hafnium and neodymium isotopes in the crust: Constraints from Precambrian crustally derived granites. *Geochim. Cosmochim. Acta* **60**, 3717–3733.
- Warren J. M. (2016) Global variations in abyssal peridotite compositions. *Lithos* **248–251**, 193–219.
- Warren J. M., Shimizu N., Sakaguchi C., Dick H. J. B. and Nakamura E. (2009) An assessment of upper mantle heterogeneity based on abyssal peridotite isotopic compositions. *J. Geophys. Res.* **114**, B12203, doi: 12210.11029/12008J B006186.
- White W. M. (1985) Sources of oceanic basalts - radiogenic isotopic evidence. *Geology* **13**, 115–118.
- White W. M. (2015a) Isotopes, DUPAL, LLSVPs, and Anekan-tavada. *Chem. Geol.* **419**, 10–28.
- White W. M. (2015b) Probing the earth's deep interior through geochemistry. *Geochem. Persp.* **4**, 95–251.
- White W. M. and Klein E. M. (2014) 4.13 - Composition of the Oceanic Crust. In *Treatise on Geochemistry (Second Edition)* (ed. H. D. H. K. Turekian). Elsevier, Oxford, pp. 457–496.
- Willbold M. and Stracke A. (2006) Trace element composition of mantle end-members: Implications for recycling of oceanic and upper and lower continental crust. *Geochem. Geophys. Geosyst.* **7**, Q04004, doi: 04010.01029/02005GC001005.
- Willbold M. and Stracke A. (2010) Formation of enriched mantle components by recycling of upper and lower continental crust. *Chem. Geol.* **276**, 188–197.
- Willig M. and Stracke A. (2019) Earth's chondritic light rare earth element composition: Evidence from the Ce–Nd isotope systematics of chondrites and oceanic basalts. *Earth Planet. Sci. Lett.* **509**, 55–65.
- Workman R. K. and Hart S. R. (2005) Major and trace element composition of the depleted mantle. *Earth Planet. Sci. Lett.* **231**, 53–72.
- Wright E. and White W. M. (1987) The origin of samoa - new evidence from Sr, Nd, and Pb isotopes. *Earth Planet. Sci. Lett.* **81**, 151–162.
- Yang S., Humayun M. and Salters V. J. M. (2018) Elemental systematics in MORB glasses from the Mid-Atlantic Ridge. *Geochem. Geophys. Geosyst.* **19**, 4236–4259, doi:4210.1029/2018GC007593.
- Zindler A. and Hart S. (1986) Chemical geodynamics. *Annu. Rev. Earth Planet. Sci.* **14**, 493–571.

Associate editor: Shichun Huang